

The chemical compositions of 10 new sub-DLAs and strong Lyman-limit systems at $z \lesssim 1.5$.

Joseph D. Meiring¹, Varsha P. Kulkarni¹, James T. Lauroesch², Celine Péroux³,
Pushpa Khare⁴, Donald G. York^{5,6}, & Arlin P. S. Crotts⁷

¹*Department of Physics and Astronomy, University of South Carolina, Columbia, SC 29208, USA*

²*Department of Physics and Astronomy, University of Louisville, Louisville, Ky 40292 USA*

³*Observatoire Astronomique de Marseille-Provence, Traverse du Siphon, Marseille, France*

⁴*Department of Physics, Utkal University, Bhubaneswar, 751004, India*

⁵*Department of Astronomy and Astrophysics, University of Chicago, Chicago, IL 60637, USA*

⁶*Enrico Fermi Institute, University of Chicago, Chicago, IL 60637, USA*

⁷*Department of Astronomy, Columbia University, New York, NY 10027, USA*

Accepted ... Received ...; in original form ...

ABSTRACT

We present chemical abundance measurements from medium resolution observations of 8 sub-damped Lyman- α absorber and 2 strong Lyman-limit systems at $z \lesssim 1.5$ observed with the MIKE spectrograph on the 6.5m Magellan II Clay telescope. These observations were taken as part of an ongoing project to determine abundances in $z_{abs} \lesssim 1.5$ quasar absorption line systems (QSOALS) focusing on sub-DLA systems. These observations increase the sample of Zn measurements in $z_{abs} \lesssim 1.5$ sub-DLAs by $\sim 50\%$. Lines of Mg I, Mg II, Al II, Al III, Ca II, Mn II, Fe II, and Zn II were detected and column densities were determined. Zn II, a relatively undepleted element and tracer of the gas phase metallicity is detected in two of these systems, with $[\text{Zn}/\text{H}] = -0.05 \pm 0.12$ and $[\text{Zn}/\text{H}] > +0.86$. The latter system is however a weak system with $N_{\text{H I}} < 18.8$, and therefore may need significant ionisation corrections to the abundances. Fe II lines were detected in all systems, with an average Fe abundance of $\langle [\text{Fe}/\text{H}] \rangle = -0.68$, higher than typical Fe abundances for DLA systems at these redshifts. This high mean $[\text{Fe}/\text{H}]$ could be due to less depletion of Fe onto dust grains, or to higher abundances in these systems. We also discuss the relative abundances in these absorbers. The systems with high metallicity show high ratios of $[\text{Mn}/\text{Fe}]$ and $[\text{Zn}/\text{Fe}]$, as seen previously in another sub-DLA. These higher values of $[\text{Mn}/\text{Fe}]$ could be a result of heavy depletion of Fe onto grains, unmixed gas, or an intrinsically non-solar abundance pattern. Based on Cloudy modeling, we do not expect ionisation effects to cause this phenomenon.

Key words: Quasars: absorption lines-ISM: abundances

1 INTRODUCTION

There are still many open questions concerning the processes of galaxy formation and evolution. Measurements of the abundances of heavy elements in galaxies give important information about the ongoing processes of star formation and death and the overall chemical enrichment of these galaxies. Studying galaxies at higher redshifts through emission is often difficult and time consuming, and biases towards more luminous galaxies are often present. Quasar absorption line systems (QSOALS) provide a means of studying the interstellar medium (ISM) of high redshift galaxies independent of the morphology of galaxies (that is, not based on the selection of galaxies of certain morphology). In addition, absorption lines in QSO spectra allow us to study the diffuse intergalactic medium using lines of O VI (e.g., Simcoe et al. 2002), or using

X-Ray absorption lines of more highly ionized species (Fang et al. 2002).

Quasar absorption line systems with strong Lyman- α lines are often divided into two classes: Damped Lyman- α (DLAs, $\log N_{\text{H I}} \geq 20.3$) and sub-Damped Lyman- α (sub-DLA $19 \lesssim \log N_{\text{H I}} < 20.3$, Péroux et al. 2001) are expected to contain a major fraction of the neutral gas in the Universe, while the majority of the baryons are thought to lie in the highly ionized and diffuse Lyman- α forest clouds with $\log N_{\text{H I}} \lesssim 14$ in intergalactic space (Petitjean et al. 1993). The DLA and sub-DLA systems are generally believed to be associated directly with galaxies, at all redshifts in which they are seen. Observations of the galaxies in emission responsible for the absorption line systems have been met with mixed results. In several instances, a galaxy at the same redshift in emission could not be found near the line of sight of the QSO (see for exam-

ple Kulkarni et al. 2000, 2001; Chen and Lanzetta 2003; Rao et al. 2003.)

DLAs have been the preferred systems for chemical abundance studies thanks to their high gas content. However, most DLAs are found to be metal poor, typically far below the solar level (e.g., Kulkarni et al. (2005) and references therein). Based on Fe II abundance measurements, Péroux et al. (2003a) suggested stronger metallicity evolution in sub-DLA systems than DLA systems. Specifically, Péroux et al. (2003a) showed that the $N_{\text{H I}}$ -weighted mean Fe metallicity in sub-DLAs increased from $\sim 1/100 Z_{\odot}$ at $z \sim 4.5$ to $\sim 1/3 Z_{\odot}$ at $z \sim 0.5$. This has been validated with Zn, the more reliable metallicity indicator by Kulkarni et al. (2007).

To date, few observations have been made of $z < 1.5$ sub-DLAs due to the lack of spectrographs with enough sensitivity at short wavelengths and the paucity of known sub-DLAs in this redshift range. Redshifts $z < 1.5$ span 70% of the age of the Universe (assuming a concordance cosmology of $\Omega_m = 0.3, \Omega_{\Lambda} = 0.7$). This redshift range is clearly important for understanding the nature of sub-DLA systems and galactic chemical evolution as well.

Recently Péroux et al. (2003a, 2006a); York et al. (2006); Kulkarni et al. (2007); Prochaska et al. (2006); Khare et al. (2007); Meiring et al. (2007) have suggested that sub-DLAs may be more metal rich than DLAs, and may contribute significantly to the cosmic metal budget. Several sub-DLA systems have actually been seen with super-solar abundances (Khare et al. 2004; Péroux et al. 2006a; Prochaska et al. 2006; Meiring et al. 2007). Super-solar abundances have also been reported in strong Lyman- α forest lines with $\log N_{\text{H I}} < 16$, although ionisation correction factors are important and not easily constrained (Charlton et al. 2003; Ding et al. 2003; Masiero et al. 2005; Schaye 2007).

As the DLA systems dominate the $N_{\text{H I}}$ weighted mean metallicity, previous studies have been dominated by DLAs. At least an equally large sample of sub-DLAs is needed to determine the overall metallicity evolution of QSO absorbers. The H I column density distribution for QSO absorbers shows that systems with $19 \lesssim \log N_{\text{H I}} \lesssim 20.3$ are ~ 8 times more numerous than the higher column density classical damped Ly α systems, making sub-DLAs more readily available probes of neutral gas in the distant Universe.

Many elements have been detected in QSO absorber systems, including C, N, O, Mg, Si, S, Ca, Ti, Cr, Mn, Fe, Ni, and Zn. Zn is often the preferred tracer of the gas-phase metallicity as it is relatively undepleted in the Galactic ISM, especially when the fraction of H in molecular form is low, as is the case in most DLAs. Zn also tracks the Fe abundance in Galactic stars (e.g., Nissen et al. (2004)), and the lines of Zn II $\lambda\lambda$ 2026, 2062 are relatively weak and typically unsaturated. These lines can be covered with ground based spectroscopy over a wide range of redshifts, $0.65 \lesssim z \lesssim 3.5$, which covers a large portion ($\sim 45\%$) of the history of the Universe. Abundances of refractory elements such as Cr and Fe relative to Zn also give a measure of the amount of dust extinction (York et al. 2006).

The number of sub-DLAs studied to date is still small, with the largest samples coming from Péroux et al. (2003a) and Meiring et al. (2007). In this paper we add 10 new systems to our previous medium-resolution measurements of sub-DLAs taken with the Magellan Inamori Kyocera Echelle (MIKE) spectrograph on the 6.5m Clay telescope at Las Campanas observatory. As the amount of published data on abundances of low redshift sub-DLAs is still small, we present these observations here with a more detailed analysis of the abundances (both absolute and relative) and

kinematics in a future paper with our complete sample. The structure of this paper is as follows. In § 2, we discuss details of our observations and data reduction techniques. In § 3, column density determinations are discussed. § 4 gives information on the individual objects, and in § 5 we discuss the abundances of these absorbers. We also provide an appendix at the end of this paper, showing plots of the UV spectra with the fits to the Lyman- α lines.

2 OBSERVATIONS AND DATA REDUCTION

The observations presented here were made with the 6.5m Magellan-II Clay telescope and the Magellan Inamori Kyocera Echelle (MIKE) spectrograph (Bernstein et al. 2003) in 2007 March. This is a double sided spectrograph with both a blue and a red camera, providing for simultaneous wavelength coverage from $\sim 3340 \text{ \AA}$ to $\sim 9400 \text{ \AA}$. Targets were observed in multiple exposures of 1800 to 2700 sec each to minimize cosmic ray defects. The seeing was typically $< 1''$, averaging $\sim 0.7''$. All of the target QSOs were observed with the $1'' \times 5''$ slit and the spectra were binned 2×3 (spatial by spectral) during readout. The resolving power of the MIKE spectrograph is $\sim 19,000$ and $\sim 25,000$ on the red and blue sides respectively with a $1''$ slit after binning. Table 1 gives a summary of the observations.

These spectra were reduced using the MIKE pipeline reduction code in IDL developed by S. Burles, J. X. Prochaska, and R. Bernstein. Wavelengths were calibrated using a Th-Ar comparison lamp taken after each exposure. The data were first bias subtracted from the overscan region and flat-fielded. The data were then sky-subtracted and the spectral orders were extracted using the traces from flat field images. These extracted spectra were then corrected for heliocentric velocities and converted to vacuum wavelengths. Each individual order was then extracted from the IDL structure created by the pipeline software and combined in IRAF using rejection parameters to reduce the effects of cosmic rays. These combined spectra were then normalized using a polynomial function to fit the continuum. These functions were typically of order five or less.

Our sample consists of 10 absorbers, 8 with $19.0 < \log N_{\text{H I}} < 20.3$ and 2 absorbers with $\log N_{\text{H I}} < 19.0$, at $z_{\text{abs}} \lesssim 1.5$, where few observations have been made to date. We selected these systems based on several criteria. Firstly, the absorbers were chosen to have $0.65 \lesssim z_{\text{abs}} \lesssim 1.5$. Faint QSOs ($m_V \lesssim 18.8$) were avoided. All absorbers have known $N_{\text{H I}}$, with $19.0 \lesssim \log N_{\text{H I}} < 20.3$. Systems that were previously known to have extremely weak lines of Mg II ($W_0^{2796} \lesssim 0.6 \text{ \AA}$), which are very unlikely to hold detectable Zn II lines at the thresholds available to this program were also excluded. Systems with low $N_{\text{H I}}$ ($N_{\text{H I}} \lesssim 19.2$) and faint QSOs ($m_V \gtrsim 18.5$) were also avoided. Throughout this paper the QSO names are given in J2000 coordinates, except in table 1 where the original name, based on J1950 coordinates is given as the name (Hewitt & Burbidge 1987).

We have attempted to be as unprejudiced as possible when selecting targets for observation. Of the ~ 45 absorbers from Rao, Turnshek, & Nestor (2006) that are accessible with MIKE (i.e. had bright enough background QSOs and were observable within the RA and declination constraints), we have observed 38 of these absorbers to date (Meiring et al. (2006, 2007), this work, and recent unpublished observations). Of the 7 that have not been observed, one was not selected because of high (yet technically possible) declination, one was excluded due to very low absorption redshift which would make detection of the Zn II lines dif-

ficult at the wavelength cutoff of MIKE, and most of the others were skipped due to scheduling and observing constraints. Only two of these 7 absorbers have $W_{2796} < 1.0 \text{ \AA}$, and none have $W_{2796} < 0.5 \text{ \AA}$ (i.e. the remaining systems are fairly strong Mg II systems), showing that this is a relatively unbiased sample. Furthermore, Kulkarni et al. (2007) showed that systems with large W_{2796} have a wide range of $[\text{Zn}/\text{H}]$, and that systems with high $[\text{Zn}/\text{H}]$ have a large range of W_{2796} , or that selection by W_{2796} in the low z $N_{\text{H I}}$ surveys does not appear to significantly bias the sample towards higher metallicity systems.

3 DETERMINATION OF COLUMN DENSITIES

Column densities were determined from profile fitting with the package FITS6P (Welty et al. 1991), which has evolved from the code by Vidal-Madjar et al. (1977). FITS6P iteratively minimizes the χ^2 value between the data and a theoretical Voigt profile that is convolved with the instrumental profile. The profile fit used multiple components, tailored to the individual system. For the central, core components, the effective Doppler parameters (b_{eff}) and radial velocities were determined from the weak and unsaturated lines, typically the Mg I λ 2852 line. For the weaker components at higher radial velocities the b_{eff} and component velocity values were determined from stronger transitions such as the Fe II $\lambda\lambda$ 2344, 2382 lines and the Mg II $\lambda\lambda$ 2796, 2803 lines. A set of b_{eff} and v values were thus determined that reasonably fit all of the lines observed in the system. The same b_{eff} values were used for all the species. The atomic data used in line identification and profile fitting are from Morton (2003).

In general, if a multiplet was observed, the lines were fit simultaneously until convergence. For all of the systems, the Fe II λ 2344, 2374, 2382 lines were fit simultaneously to determine a set of column densities that fit the spectra reasonably well. Similarly, the Mg II $\lambda\lambda$ 2796, 2803 lines were also fit together. Significant saturation of the Mg II $\lambda\lambda$ 2796, 2803 and Al II λ 1670 lines allowed for only lower limits to be placed on the column densities for these species. The Zn II λ 2026.137 line is blended with a line of Mg I λ 2026.477. The Mg I contribution to the line was estimated using the Mg I λ 2852 line, for which $f\lambda$ is ~ 32 times that of the Mg I λ 2026 line. The Zn II components were then allowed to vary while the Mg I components were held fixed. $N_{\text{Cr II}}$ was determined by simultaneously fitting the Cr II λ 2056 line and the blended Cr II + Zn II λ 2062 line, where the contribution from Zn II was estimated from the Zn II + Mg I λ 2026 line. See also Khare et al. (2004) and Meiring et al. (2007) for a discussion of the profile fitting scheme. In this paper we adopt the standard notation:

$$[X/Y] = \log(N_X/N_{\text{H I}}) - \log(X/\text{H})_{\odot} \quad (1)$$

Solar system abundances have been adopted from Lodders (2003).

We present the rest-frame equivalent widths (W_0) of the lines in Table 2. The 1σ errors for the equivalent widths are given also and reflect both uncertainties in the continuum level and in the photon noise. If a certain line was not detected, the limiting equivalent width was determined from the local signal to noise ratio (S/N) and uncertainties in the continuum placement based on a 3-pixel element. Assuming a linear curve of growth, a corresponding 3σ upper limit was also placed on the column density.

We give total column densities (the sum of the column densities in the individual components determined via profile fitting method) for these systems in table 3. Column densities were also

obtained via the apparent optical depth (AOD) method as a consistency check, and are also listed in table 3. For a discussion of the AOD method, see Savage & Sembach (1996). Errors for the AOD column densities include contributions from both the photon noise and continuum placement. In most cases, the column densities from the profile fitting and AOD methods agree to within the error bars, especially for the weak and unsaturated lines.

4 DISCUSSION OF INDIVIDUAL OBJECTS

4.1 Q1037+0028 ($z_{em} = 1.733$)

(System A: $z_{abs}=1.4244$): This QSO harbors a sub-DLA with $\log N_{\text{H I}} = 20.04 \pm 0.12$ (Rao, Turnshek, & Nestor 2006). We detected absorption lines for Mg II, Al II, Al III, Si II, Mn II and Fe II in this sub-DLA system. The Mg I λ 2852 line was blended with telluric features at $\sim 6916 \text{ \AA}$. A total of 11 components were used in the profile fitting for this system. No Zn II lines were detected in this system at $S/N \sim 16$ in the region, and a limiting EW of $W_0 < 21 \text{ m\AA}$. There were two small features that lined up with the components at 11 and 44 km s^{-1} from other lines, however, the equivalent width of the features was significant at only a $\lesssim 2\sigma$ level. Total column densities for this and all other systems are given in Table 3. The abundance based on Fe lines was $[\text{Fe}/\text{H}] = -0.67 \pm 0.12$. This system shows $\text{Al III}/\text{Al II} < -0.96$, a typical level of ionisation for a sub-DLA (e.g., Dessauges-Zavadsky et al. (2003); Meiring et al. (2007)). Rest frame equivalent widths for the lines in this system are found in table 2, along with the results of the profile fitting in table 4. Velocity plots of several lines of interest are shown in Figure 1.

There also appears to be a weaker system at $z_{abs}=0.6572$, with $W_0(\text{Mg II } 2796)=354 \text{ m\AA}$. We detect the Fe II $\lambda\lambda$ 2344, 2382, 2586, and 2600 lines along with the Mg I λ 2852 line as well. The Fe II λ 2374 line is blended with the Galactic Ca II λ 3934 line for this system. $N_{\text{H I}}$ cannot be determined for this weaker system due to the break in the continuum from the sub-DLA system at $z_{abs}=1.4244$ beyond the Lyman limit, so it is not included in our sample (which depends on known $N_{\text{H I}}$, as noted earlier).

4.2 Q1054-0020 ($z_{em}=1.021$)

(System A: $z_{abs}=0.8301$): System A is a strong Lyman-limit system with $N_{\text{H I}}=18.95 \pm 0.18$ (Rao, Turnshek, & Nestor 2006). Five components were used in the profile fits for system A. Lines of Mg I, Mg II, Mn II, and Fe II were all detected. No Zn II lines were seen at $S/N \sim 23$ in the region, We did not detect Zn II λ 2026 with a limiting EW of $W_0 < 10 \text{ m\AA}$, and $[\text{Zn}/\text{H}] < +0.18$. This system has a ratio of $N_{\text{Fe II}}/N_{\text{H I}} = -0.09 \pm 0.18$ dex. The true ratio may be lower due to ionisation (see our later comments on ionisation corrections at low $N_{\text{H I}}$). We also detected lines of Mn II $\lambda\lambda$ 2576, 2594 with $[\text{Mn}/\text{Fe}] = -0.09 \pm 0.07$. The Al II λ 1670 line lies below the wavelengths covered by MIKE, so the Al III/Al II ratio could not be measured in this system. We did however detect strong Al III $\lambda\lambda$ 1854, 162 lines. Velocity plots of several lines of interest are shown in Figure 2. Rest frame equivalent widths for the lines in this system can be found in table 2, with the results of the profile fitting analysis in table 5.

(System B: $z_{abs}=0.9514$): A total of 7 components were used to fit system B with $N_{\text{H I}}=19.28 \pm 0.02$ (Rao, Turnshek, & Nestor

Table 1. Summary of observed targets and their absorption systems.

QSO	Alternate name or SDSS ID	mV or g	RA	Dec	z_{em}	z_{abs}	$\log N_{\text{H I}}$	$E(B-V)_{g-i}^a$	Exposure time	Reference
J2000			J2000	J2000			cm^{-2}		s	
Q1037+0028	SDSS J103744.44+002809.2	18.4	10:37:44.40	+00:28:09.2	1.733	1.4244	20.04 ± 0.12	0.04	10800	1
Q1054-0020	SDSS J105440.98-002048.4	18.3	10:54:40.98	-00:20:48.4	1.021	0.8301	18.95 ± 0.18	... ^b	10800	1
...	0.9514	19.28 ± 0.02	0.05
Q1215-0034	Q1213-002	17.0	12:15:49.81	-00:34:32.1	2.691	1.5543	19.56 ± 0.02	0.02	5400	2
Q1220-0040	SDSS J122037.00-004032.4	18.5	12:20:37.00	-00:40:32.4	1.411	0.9746	20.20 ± 0.07	-0.02	8100	1
Q1228+1018	Q1226+105	18.5	12:28:36.80	+10:18:41.7	2.305	0.9376	19.41 ± 0.15	0.00	7200	3
Q1330-2056	Q1327-206	17.0	13:30:07.70	-20:56:16.4	1.165	0.8526	19.40 ± 0.02	N/A ^c	3600	4,5
Q1436-0051	SDSS J143645.06-005150.6	18.5	14:36:45.03	-00:51:50.6	1.275	0.7377	20.08 ± 0.11	0.08	5400	1
...	0.9281	<18.8	... ^b
Q1455-0045	SDSS J145508.14-004507.4	18.0	14:55:08.14	-00:45:07.5	1.378	1.0929	20.08 ± 0.06	0.02	8100	1

REFERENCES: (1) Nestor (2004); (2) Lanzetta, Turnshek, & Wolfe (1987); (3) Barthel, Tytler, & Thompson (1990); (4) Kunth & Bergeron (1984); (5) Bergeron, Kunth, & D’Odorico (1987)

^aDetermined using the colour excess $\Delta(g-i) = (g-i) - (g-i)_{med}$, where $(g-i)_{med}$ is the median QSO colour at the emission redshift from Richards et al. (2001) and the relation $E(B-V)_{g-i} = \Delta(g-i)(1+z_{abs})^{-1.2}/1.506$ (Khare et al. 2004; York et al. 2006).

^bThe extinction is attributed to the system with the higher $N_{\text{H I}}$, although the true extinction could be due to either, or both systems.

^cThis QSO was not observed in the SDSS

2006). Only lines of Mg I, Mg II, and Fe II were detected in this system. We were able to constrain the metallicity of this system based on the non detection of the Zn II λ 2026 line to be $[\text{Zn}/\text{H}] < -0.21$ with $S/N \sim 30$ in the region. This system also has a low metallicity based on Fe with $[\text{Fe}/\text{H}] = -1.09 \pm 0.02$, although dust depletion may be important. The Al II λ 1670 line lies below the covered wavelengths. The Al III $\lambda\lambda$ 1854, 1862 lines were covered but not detected with $W_0 < 22 \text{ m}\text{\AA}$. Velocity plots of several lines of interest are shown in Figure 3. The results of the profile fitting analysis are found in table 6, and the rest frame equivalent widths for the lines in this system in table 2.

4.3 Q1215-0034 ($z_{em}=2.691$)

(System A: $z_{abs}=1.5543$): This fairly high redshift QSO harbors a sub-DLA with $\log N_{\text{H I}} = 19.56 \pm 0.02$ (Rao, Turnshek, & Nestor 2006). Fourteen components were used in the profile fit for this system, spanning $\sim 390 \text{ km s}^{-1}$ in velocity space. Several of the components were detected only in the Mg II $\lambda\lambda$ 2796, 2803 lines. We detected lines from Mg II $\lambda\lambda$ 2796, 2803 and Fe II $\lambda\lambda$ 2344, 2374, 2382, 2586, and 2600. The Al II λ 1670 and Al III $\lambda\lambda$ 1854, 1862 lines were covered, but are blended with features inside the Lyman- α forest. The Mg I λ 2852 line was blended with telluric features at $\sim 7284 \text{ \AA}$. We did not detect Zn II at $S/N \sim 30$ in the region, but we could place an upper limit of $[\text{Zn}/\text{H}] < -0.56$, and based on the Fe II lines an abundance of $[\text{Fe}/\text{H}] = -0.64 \pm 0.02$. Velocity plots of lines of interest are shown in Figure 4. The results of the profile fitting analysis are given in table 7, with the rest frame equivalent widths for the lines in this system in table 2.

4.4 Q1220-0040 ($z_{em}=1.411$)

(System A: $z_{abs}=0.9746$): There is a sub-DLA with $\log N_{\text{H I}} = 20.20 \pm 0.07$ in the UV spectrum of this QSO (Rao, Turnshek, & Nestor 2006). We detect lines of Al III, Mg I, Mg II, and Fe II in this sub-DLA. A total of 9 components

were used to fit the line profiles for this system. The Al II λ 1670 line lies below the wavelengths accessible to MIKE, so we were unable to determine the Al III/Al II ratio for this system. Al III was detected only in the components at $v = -197$ and $v = -162 \text{ km s}^{-1}$, and not in the components where other ions were the bulk of the absorption from other ions was seen, such as the $v=2$, $v=38$, or $v=74 \text{ km s}^{-1}$ components. We did not detect any Zn II lines in this system at $S/N \sim 23$ in the region, and place an upper limit on the Zn metallicity of $[\text{Zn}/\text{H}] < -1.14$. The Fe II abundance is similarly low for this system, with $[\text{Fe}/\text{H}] = -1.33 \pm 0.07$. We show velocity plots of several lines in Figure 5. The results of the profile fitting analysis are found in table 8, with the rest frame equivalent widths for this system in table 2.

4.5 Q1228+1018 ($z_{em}=2.305$)

(System A: $z_{abs}=0.9376$): This moderately high redshift QSO has a sub-DLA in its spectrum with $\log N_{\text{H I}} = 19.41 \pm 0.02$ (Rao, Turnshek, & Nestor 2006). We detected strong lines of Mg I, Mg II, and Fe II in this sub-DLA. A total of 9 components were used in the Voigt profile fits. Due to the high redshift of the background QSO, several lines were blended with Lyman- α forest clouds, such as Al III $\lambda\lambda$ 1854, 1862 and Si II λ 1808. The Zn II $\lambda\lambda$ 2026, 2062 lines also fell inside the Lyman- α forest, but lay between strong absorption features, especially the Zn II λ 2026 line. There is a strong forest line in the blue end of the expected position of the Zn II feature, as can be seen in the velocity plots in Figure 6, however the components which are most likely to hold Zn II are at $v=2$, $v=26$, and $v=51 \text{ km s}^{-1}$, which are unblended. Nonetheless, no Zn II is seen, and we place an upper limit on the Zn metallicity of $[\text{Zn}/\text{H}] < -0.37$ with $S/N \sim 26$ in the region. The Fe abundance for this sub-DLA is high compared to typical DLA Fe abundances, with $[\text{Fe}/\text{H}] = -0.30 \pm 0.02$. The results of the profile fitting analysis are given in table 9, with the rest frame equivalent widths for the lines in this system given in table 2.

Table 2. Rest-frame equivalent widths of key metal lines. Values and 1σ errors are in units of mÅ.

QSO	z_{abs}	Mg I 2852	Mg II 2796	Mg II 2803	Al II 1670	Al III 1854	Al III 1862	Si II 1526	Si II 1808	Ca II 3933	Ca II 3969	Cr II 2056
Q1037+0028	1.4244	- ^a	2443±19	2054±32	677±15	169±12	87± 8	746±49	60±9	-	-	<7
Q1054-0020	0.8301	350±15	1180±14	1077±12	-	415±18	287±28	-	-	-	-	<11
	0.9514	131±22	769±19	542±27	-	<22	<11	-	<11	-	-	<6
Q1215-0034	1.5543	-	1987±21	1543±26	-	-	-	-	-	-	-	<10
Q1220-0040	0.9746	152±20	1919±32	1688±32	-	71± 22	40± 22	-	-	-	-	<9
Q1228+1018	0.9376	245±38	1678±40	1457±23	-	-	-	-	-	-	-	<6
Q1330-2056	0.8526	293±66	2413±64	1807±41	-	75± 24	26± 19	-	-	-	-	<6
Q1436-0051	0.7377	583±14	1113±10	1081±13	-	-	-	-	-	396±15	-	<20
	0.9281	233±21	1105±40	867±33	-	220±22	156±22	-	46± 9	122±17	-	<16
Q1455-0045	1.0929	363±21	1659±10	1586±11	804±14	515±15	281±17	-	-	-	-	21 ± 7
QSO	z_{abs}	Mn II 2576	Mn II 2594	Mn II 2606	Fe II 2260	Fe II 2344	Fe II 2374	Fe II 2382	Fe II 2586	Fe II 2600	Zn II 2026	Zn II 2062
Q1037+0028	1.4244	75±20	82±18	40± 13	93±21	963±61	507±21	1442±55	839±51	1427±41	<21	<15
Q1054-0020	0.8301	42±11	39±8	<8	<7	586±7	277±9	805±6	548±6	831±6	<10	<15
Q1054-0020	0.9514	<18	<10	<13	<6	198±15	45± 9	420±18	208±27	453±27	<9	<13
Q1215-0034	1.5543	<9	<8	<7	24±5	507±14	267±9	861±20	449±10	896±24	<8	<10
Q1220-0040	0.9746	<19	<22	<17	<8	624±10	278±10	1049±32	566±25	932±22	<9	<9
Q1228+1018	0.9376	<29	<20	<18	64±12	692±12	417±22	989±9	660±19	1032±26	<9	<8
Q1330-2056	0.8526	<9	<8	<8	<6	271±51	58± 43	803±43	204±41	784±40	<16	<6
Q1436-0051	0.7377	207±17	134±14	85±15	116±24	757±17	580±16	847±9	785±11	926±16	108±12	101 ± 35
	0.9281	43±16	<22	102±32	25±7	341±16	189±13	501±13	307±36	471±23	26± 7	<21
Q1455-0045	1.0929	29±6	50±14	<19	<12	902±11	470±22	1135±14	874±24	1226±21	<15	<8

^aBlank entries indicate that the line was not measured due to lack of wavelength coverage, extremely low S/N at the wavelength extremes, or blends with telluric features.

Table 3. Total column densities for the systems observed. Values are logarithmic, in units of cm^{-2} .

QSO	z_{abs}	$\log N_{\text{H I}}$	Mg I	Mg II	Al II	Al III	Si II	Ca II	Ti II	Cr II	Mn II	Fe II	Zn II
Q1037+0028	1.4244	20.04 ± 0.12	-	>15.48	>14.15	13.19 ± 0.02	15.09 ± 0.03	-	-	<12.26	12.53 ± 0.05	14.84 ± 0.02	<12.04
AOD				>14.44	>13.60	13.15 ± 0.03	15.05 ± 0.05				12.57 ± 0.11	14.96 ± 0.09	
Q1054-0020A	0.8301	18.95 ± 0.18	12.55 ± 0.01	>14.83	-	13.59 ± 0.06	-	-	-	<12.47	12.27 ± 0.07	14.33 ± 0.01	<11.76
AOD			12.54 ± 0.02	>14.30		13.65 ± 0.04					12.31 ± 0.10	14.35 ± 0.01	
Q1054-0020B	0.9514	19.28 ± 0.02	12.04 ± 0.03	>13.72	-	<12.11	<14.25	-	<12.36	<12.20	<11.92	13.66 ± 0.01	<11.70
AOD			12.04 ± 0.07	>13.59								13.49 ± 0.08	
Q1215-0034	1.5543	19.56 ± 0.02	-	>15.34	-	-	-	-	-	<12.37	<11.63	14.39 ± 0.01	<11.63
AOD				>14.25								14.35 ± 0.11	
Q1220-0040	0.9746	20.20 ± 0.07	12.12 ± 0.03	>14.81	-	12.62 ± 0.06	-	-	<12.47	<12.38	<11.95	14.34 ± 0.02	<11.69
AOD			12.10 ± 0.05	>14.37		12.68 ± 0.12						14.35 ± 0.01	
Q1228+1018	0.9376	19.41 ± 0.02	12.32 ± 0.04	>14.61	-	-	-	-	<11.65	<12.21	<12.14	14.58 ± 0.01	<11.67
AOD			12.32 ± 0.05	>14.36								14.55 ± 0.02	
Q1330-2056	0.8526	19.40 ± 0.02	12.33 ± 0.03	>14.21	-	12.59 ± 0.05	-	-	<11.45	<12.18	<11.61	13.80 ± 0.01	<11.96
AOD			12.37 ± 0.09	>14.12		12.52 ± 0.15						13.76 ± 0.07	
Q1436-0051A	0.7377	20.08 ± 0.11	>12.92	>14.42	-	-	-	12.83 ± 0.02	<11.71	<12.71	13.01 ± 0.02	14.94 ± 0.02	12.67 ± 0.05
AOD			>12.90	>14.26				12.79 ± 0.01			13.05 ± 0.03	14.92 ± 0.02	12.80 ± 0.05
Q1436-0051B	0.9281	<18.8	12.49 ± 0.04	>15.12	-	13.40 ± 0.03	15.02 ± 0.05	12.28 ± 0.04	<12.71	<12.59	12.45 ± 0.05	14.20 ± 0.01	12.29 ± 0.06
AOD			12.45 ± 0.03	>14.11		13.31 ± 0.03	14.97 ± 0.07	12.15 ± 0.05			12.32 ± 0.07	14.25 ± 0.02	12.23 ± 0.05
Q1455-0045	1.0929	20.08 ± 0.06	12.53 ± 0.02	>14.92	>13.83	13.65 ± 0.02	14.64 ± 0.10	-	<12.44	12.40 ± 0.13	12.09 ± 0.15	14.57 ± 0.01	<11.91
AOD			12.51 ± 0.02	>14.45	>13.71	13.67 ± 0.01	14.84 ± 0.12			12.75 ± 0.17	12.20 ± 0.10	14.61 ± 0.02	

Table 4. Column densities for the $z = 1.4244$ absorber in Q1037+0028 with $N_{\text{H I}} = 20.04 \pm 0.12$. Velocities and b_{eff} values are in units of km s^{-1} , and column densities are in units of cm^{-2} . Errors in the column densities are the 1σ values.

v	b_{eff}	Mg II	Al II	Al III	Si II	Mn II	Fe II
-158	6.9	> 3.14E13	> 2.34E12	(6.59±1.40)E11	(4.26±0.59)E13	-	(1.63±0.13)E13
-118	5.9	> 8.37E13	> 2.16E12	-	(5.69±0.98)E13	-	(3.04±0.21)E13
-91	6.7	> 3.91E12	> 4.06E11	-	(6.52±0.20)E12	-	(2.92±0.76)E12
-57	13.5	> 1.65E13	> 1.28E12	-	(3.65±0.46)E13	-	(1.65±0.14)E13
-40	6.9	> 9.77E11	> 1.47E12	-	(2.98±0.60)E13	-	(1.69±0.17)E13
-19	10.0	> 6.90E13	> 4.60E12	(1.37±0.17)E12	(7.21±0.93)E13	-	(3.92±0.21)E13
11	8.1	> 1.23E14	> 5.88E13	(1.12±0.05)E13	(7.10±0.61)E14	(2.07±0.29)E12	(3.08±0.25)E14
44	7.9	> 2.69E15	> 6.80E13	(2.42±0.18)E12	(2.53±0.48)E14	(1.33±0.26)E12	(2.36±0.17)E14
100	11.2	> 7.16E12	(4.64±0.98)E11	-	(6.79±2.23)E12	-	(5.65±0.89)E12
147	12.6	> 1.56E13	(9.89±1.16)E11	-	(2.43±0.32)E13	-	(1.33±0.11)E13
183	4.6	> 4.57E12	-	-	-	-	-

Table 5. Same as table 3, but for the $z_{abs}=0.8301$ system in Q1054-0020 with $N_{\text{H I}} = 18.95 \pm 0.18$.

v	b_{eff}	Mg I	Mg II	Al III	Mn II	Fe II
-25	9.1	(4.53±0.41)E11	>1.07E14	(9.41±1.86)E12	-	(3.07±0.08)E13
2	10.3	(1.53±0.08)E12	>2.00E14	(1.80±0.43)E13	(8.30±1.68)E11	(7.96±0.20)E13
19	8.1	(6.91±0.58)E11	> 8.82E12	-	(4.12±1.50)E11	(2.63±0.10)E13
49	13.4	(8.89±0.51)E11	> 3.59E14	(1.15±0.18)E13	(6.09±1.73)E11	(7.94±0.15)E13
104	15.8	-	(1.23±0.12)E12	-	-	-

Table 6. Same as table 3, but for the $z_{abs}=0.9514$ system in Q1054-0020 with $N_{\text{H I}} = 19.28 \pm 0.02$.

v	b_{eff}	Mg I	Mg II	Fe II
-447	8.0	-	(1.15±0.11)E12	-
-90	5.1	(1.71±0.28)E11	>6.74E12	(4.86±0.27)E12
-71	4.6	-	>1.84E12	-
-13	10.0	(2.23±0.31)E11	>1.24E13	(9.84±0.34)E12
49	3.5	(7.26±2.45)E10	>1.43E12	(1.71±0.23)E12
72	8.0	(5.24±0.41)E11	>2.64E13	(2.66±0.06)E13
87	10.3	(1.07±0.33)E11	>3.07E12	(2.69±0.33)E12

Table 7. Same as table 3, but for the $z_{abs}=1.5543$ system in Q1215-0034 with $N_{\text{H I}} = 19.56 \pm 0.02$.

v	b_{eff}	Mg II	Fe II
-271	8.0	(1.42±0.09)E12	-
-217	6.7	(1.84±0.10)E12	-
-188	9.7	>7.93E12	(2.52±0.41)E12
-154	9.0	>1.10E13	(2.28±0.40)E12
-131	7.4	>1.04E12	-
-103	13.9	>1.77E12	-
-75	8.7	>5.48E12	(5.22±0.44)E12
-45	10.0	>3.30E13	(1.75±0.06)E13
-3	9.7	>2.06E15	(9.13±0.36)E13
14	15.5	>6.78E13	(1.18±0.03)E14
42	10.9	>1.57E13	(6.80±0.61)E12
70	10.9	(2.92±0.13)E12	-
102	5.4	(1.16±0.09)E12	-
120	6.2	(1.87±0.10)E12	(1.77±0.37)E12

Table 8. Same as table 3, but for the $z_{abs}=0.9746$ system in Q1220-0040 with $N_{HI}=20.20\pm 0.07$.

v	b_{eff}	Al III	Mg I	Mg II	Fe II
-197	4.9	(1.50±0.33)E12	-	>6.51E12	(1.03±0.27)E12
-162	5.6	(2.70±0.42)E12	-	>1.53E13	-
-135	11.1	-	-	>4.45E12	-
-100	4.6	-	-	>4.19E12	(2.08±0.29)E12
-45	8.0	-	-	>3.10E12	(1.52±0.32)E12
2	14.6	-	(6.71±0.52)E11	>4.95E14	(1.22±0.02)E14
38	15.8	-	(3.91±0.48)E11	>5.58E13	(4.91±0.11)E13
75	15.2	-	(2.59±0.44)E11	>5.86E13	(4.08±0.09)E13
106	9.0	-	-	>6.07E12	(2.60±0.36)E12

Table 9. Same as table 3, but for the $z_{abs}=0.9376$ system in Q1228+1018 with $N_{HI}=19.41\pm 0.02$.

v	b_{eff}	Mg I	Mg II	Fe II
-44	20.2	-	(3.05±0.27)E12	(3.05±0.58)E12
-15	8.9	(2.16±0.69)E11	>6.96E13	(1.86±0.08)E13
2	9.2	(1.18±0.66)E11	>2.46E13	(3.97±0.14)E13
26	9.9	(9.72±1.02)E11	>1.64E14	(2.29±0.05)E14
51	11.1	(4.93±0.78)E11	>6.42E13	(3.95±0.12)E13
77	8.0	(1.88±0.61)E11	>5.86E13	(4.31±0.13)E12
109	7.4	-	>1.39E13	(6.54±0.45)E12
126	4.9	(1.04±0.36)E11	>8.37E12	(1.72±0.38)E12
155	14.9	-	(4.17±0.25)E12	(1.92±0.48)E12

4.6 Q1330-2056 ($z_{em}=1.165$)

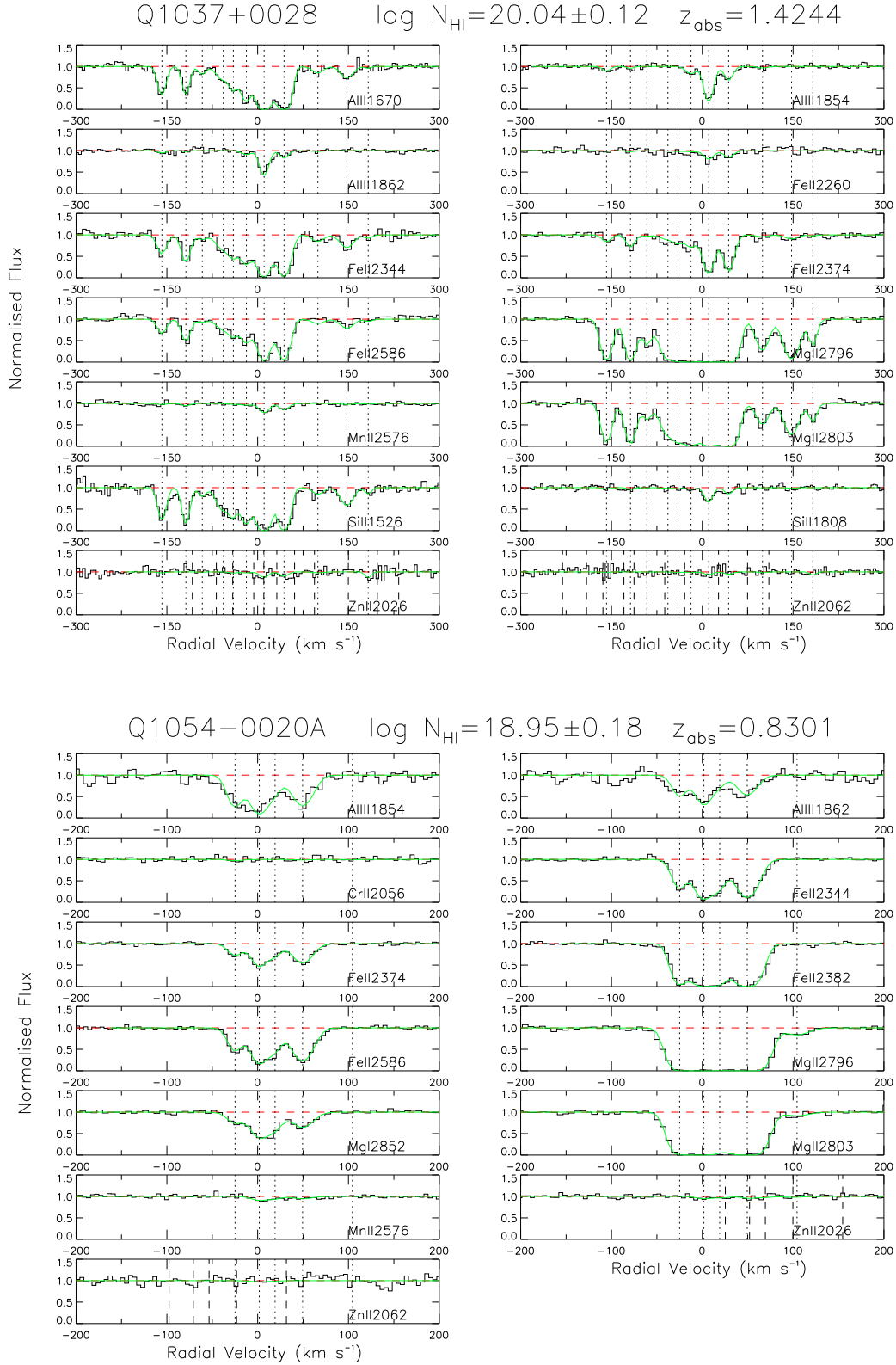
(System A: $z_{abs}=0.8526$): In the spectrum of this relatively bright ($m_V = 17.0$) QSO, there is a sub-DLA at $z_{abs}=0.8526$ with $\log N_{HI}=19.40\pm 0.02$ (Rao, Turnshek, & Nestor 2006). We detected strong absorption from Al III, Mg I, Mg II, and Fe II. The Al II λ 1670 line was below the covered wavelengths, so the Al III/Al II ratio could not be determined for this system. This system required 15 components in the Voigt profile models for an adequate fit. The components spanned ~ 650 km s $^{-1}$ in velocity space. The Zn II λ 2026 line fell near a bad column in the CCD on the blue side. However, the components where Zn II is most likely, such as the components with the strongest Mg I absorption, are outside of the affected area. We have highlighted the affected area in grey in the plot of the Zn II λ 2026 line in Figure 7. No Zn II was detected, and an upper limit of $[Zn/H] < -0.07$ was placed on the system at $S/N \sim 18$ in the region. The Fe abundance was low, with $[Fe/H] < -1.07\pm 0.02$. We give velocity plots of several lines in Figure 7. The results of the profile fitting analysis are shown in table 10, with the rest frame equivalent widths for the lines in this system given in table 2.

4.7 Q1436-0051 ($z_{em}=1.275$)

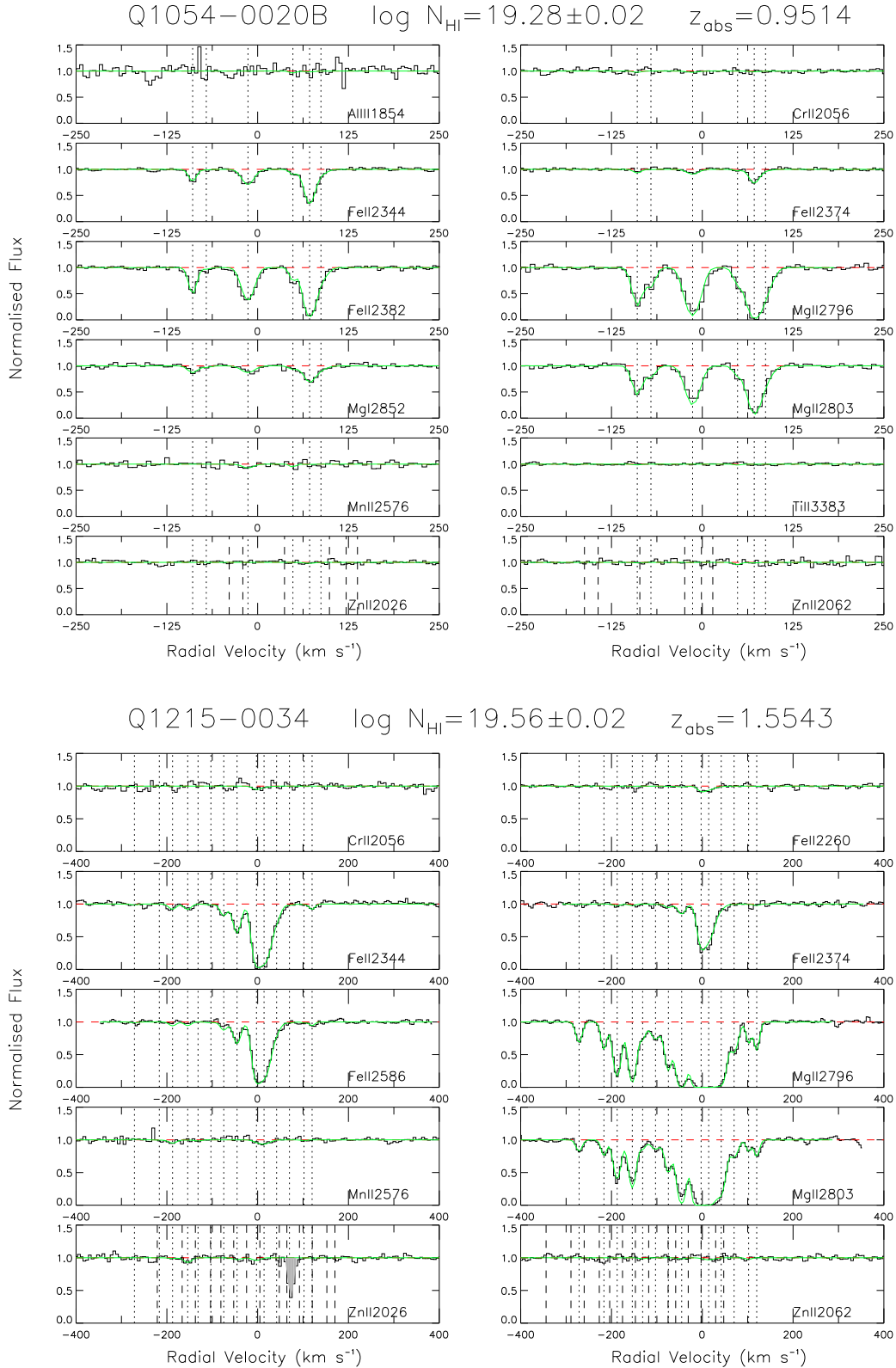
(System A: $z_{abs}=0.7377$): This is a sub-DLA system with $\log N_{HI}=20.08\pm 0.11$ (Rao, Turnshek, & Nestor 2006). We detect absorption lines from Mg I, Mg II, Ca II, Mn II, Fe II, and Zn II in system A. A total of 8 components were used to fit the absorption profiles. There is also a C IV system at $z_{abs}=1.2699$, with the C IV λ 1550 line close to the expected position of the Zn II λ

2026 line in the sub-DLA at $z_{abs}=0.7377$, as can be seen in the velocity plots shown in Figure 8. The C IV $\lambda\lambda$ 1548, 1550 lines were fit simultaneously, and later held fixed while fitting the Zn II $\lambda\lambda$ 2026, 2062 lines simultaneously. The C IV system shows a simple structure with only 2 components needed to fit the profile, with no absorption in the region where the majority of the Zn II λ 2026 absorption is. In Figure 8, the C IV contribution to this line is highlighted in grey. The Mg I contribution to the Zn II λ 2026 line, based on the fit to the Mg I 2852 line, was also included and held fixed. This was the only case of an appreciable contribution of Mg I to the blended Zn II + Mg I λ 2026 line that was seen. This system has a high metallicity with $[Zn/H] = -0.05\pm 0.11$, and $[Fe/H] = -0.61\pm 0.11$. We also detect strong Mn II $\lambda\lambda$ 2576, 2594, 2606 lines with $[Mn/H] = -0.57\pm 0.11$ and $[Mn/Fe] = +0.04\pm 0.03$. The Ca II λ 3934 line was detected with $W_0=396\pm 15$ mÅ, but the Ca II λ 3969 line was blended with telluric features. The Si II λ 1808 line was not observable for this sub-DLA, so no information on α -enhancement is available for this system. We show the results of the profile fitting analysis in table 11, and give the rest frame equivalent widths for this system in table 2.

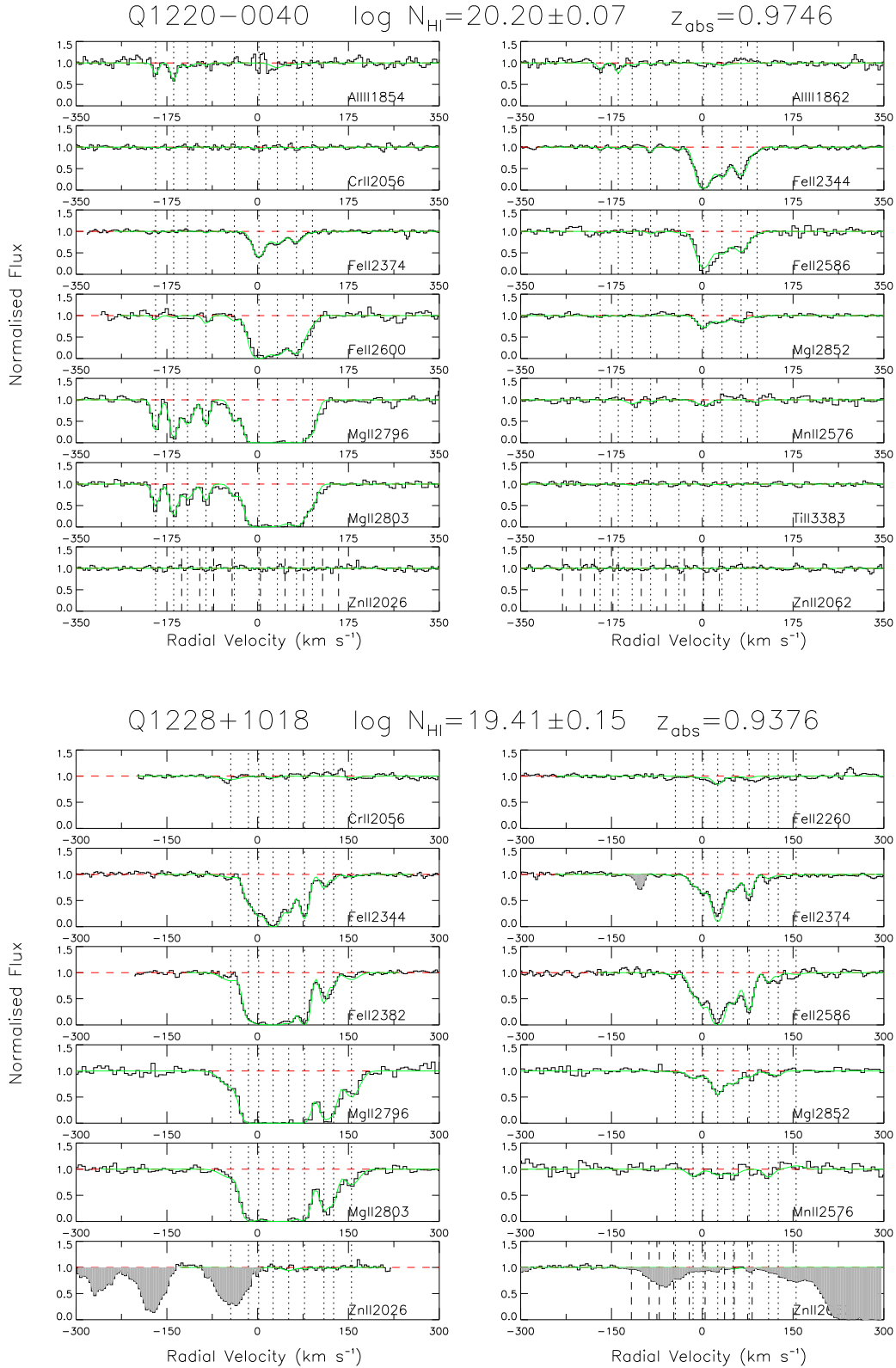
(System B: $z_{abs}=0.9281$): This is a Lyman-limit system with $\log N_{HI} < 18.8$ (Rao, Turnshek, & Nestor 2006). Several lines are detected in this system, such as Mg I, Mg II, Al III, Si II, Ca II, Mn II, and Fe II. A total of 6 components were used in the Voigt profile fits for this system, although Si II, Ca II, and Zn II were only detected in the $v \sim 9$ km s $^{-1}$ component. This system has a large amount of Al III and likely has a high degree of ionisation, although the Al II λ 1670 line was not in the wavelengths covered. The Ca II λ 3969 line was again blended with telluric features. The Fe II λ 2344 line is partly contaminated by the Fe II λ 2600 line from system A.



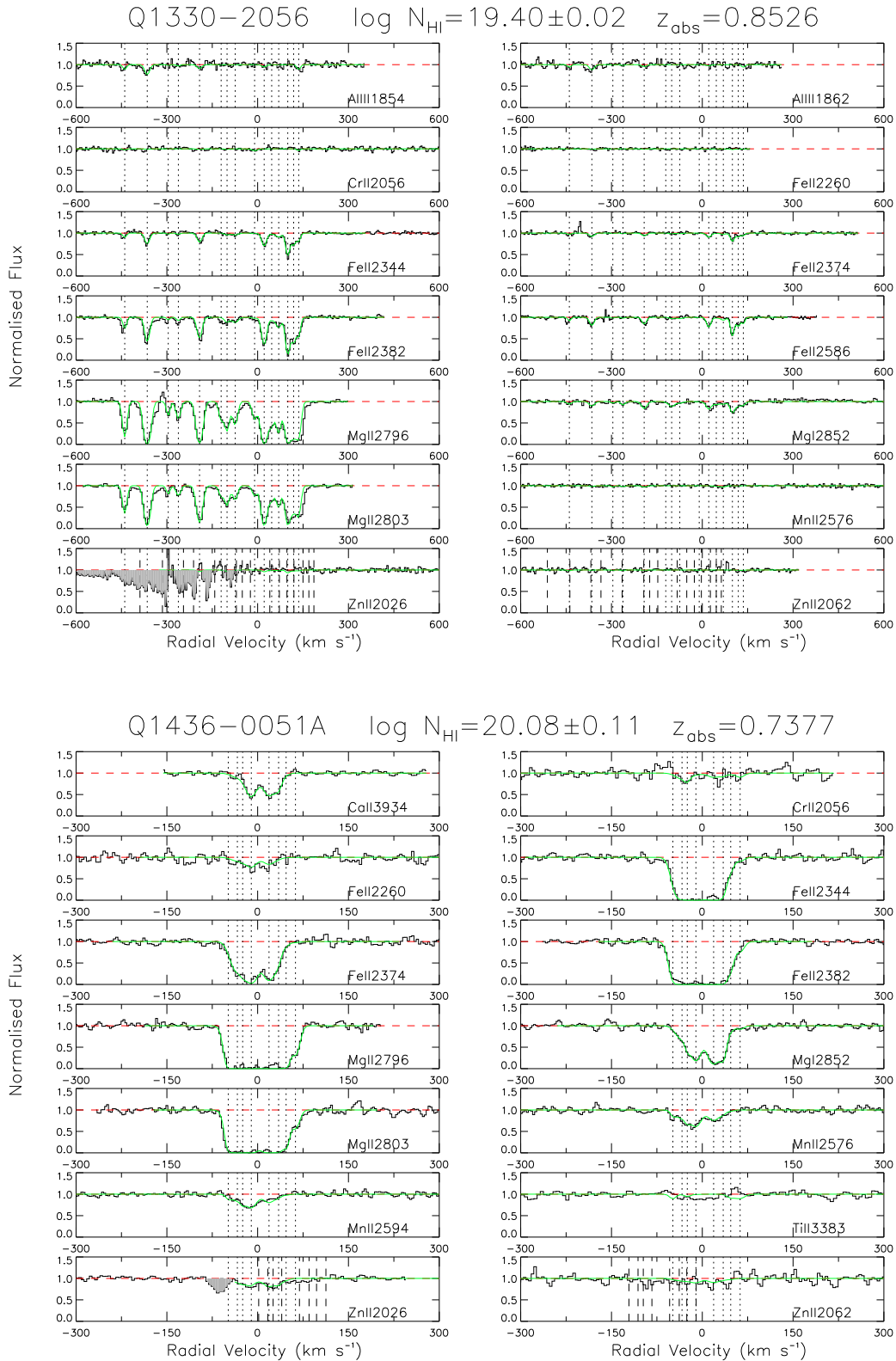
Figures 1 and 2: Velocity plots for several lines of interest in the $z = 1.4244$ system (top) in the spectrum of Q1037+0028 and the $z_{\text{obs}} = 0.8301$ system in Q1054-0020 (system A, bottom). The solid green line indicates the theoretical profile fit to the spectrum, and the dashed red line is the continuum level. The vertical dotted lines indicate the positions of the components that were used in the fit. In the cases of the Zn II $\lambda\lambda$ 2026, 2062 lines, which have other lines nearby, the long dashed vertical lines indicate the positions of the components for Mg I (former case), and Cr II (latter case).



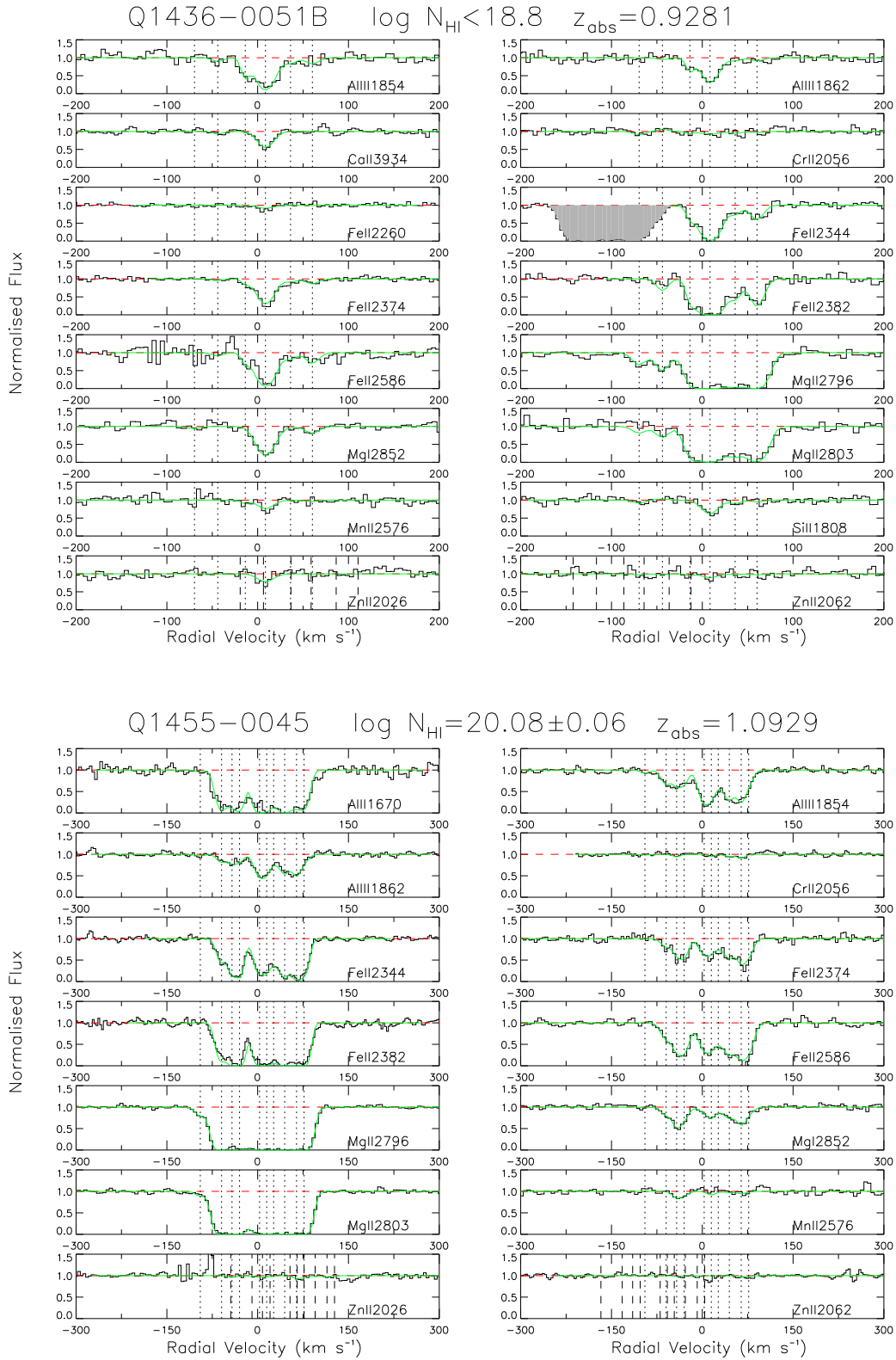
Figures 3 and 4: Same as Figure 1, but for the $z_{\text{abs}}=0.9514$ system in Q1054-0020 (system B, top), and the $z_{\text{abs}}=1.5543$ system in Q1215-0034 (bottom). For the $z_{\text{abs}}=1.5543$ system in Q1215-0034, the area shaded in grey in the panel displaying the Zn II λ 2026 line is an unidentified feature, not due to absorption from Zn II. This may be due to Mg I 2026, however, the Mg I 2852 line was blended with telluric features, and we could therefore not estimate the Mg I contribution to this line.



Figures 5 and 6: Same as Figure 1, but for the $z_{\text{abs}} = 0.9746$ system in Q1220-0040 (top), and the $z_{\text{abs}} = 0.9376$ system in Q1228+1018 (bottom). The areas shaded in grey in the Zn II λ 2026, 2062 panels for the $z_{\text{abs}} = 0.9376$ system in Q1228+1018 represent absorption from lines inside the Lyman- α forest, and are not due to absorption from Zn II. There is a small, unidentified feature near the Fe II λ 2374 line, which has also been shaded in grey.



Figures 7 and 8: Same as Figure 1, but for the $z_{\text{abs}}=0.8526$ system in Q1330-2056 (top), and the $z_{\text{abs}}=0.7377$ system in Q1436-0051 (system A, bottom). For the $z_{\text{abs}}=0.8526$ system in Q1330-2056, in the region around the expected position of Zn II λ 2026, there is a bad column in the blue CCD that caused the feature seen in the figure. The part of the profile that is affected by the bad column is shaded in grey to highlight this defect. For the $z_{\text{abs}}=0.7377$ system in Q1436-0051, we have highlighted the contribution of the C IV λ 1550 line at $z_{\text{abs}}=1.2699$ to the Zn II 2026 profile in grey. See § 4.7 for a discussion of this blend.



Figures 9 and 10: Same as Figure 1, but for the $z_{\text{abs}}=0.9281$ system in Q1436-0051 (system B, top), and the $z_{\text{abs}}=1.0929$ system in Q1455-0045 (bottom).

Table 10. Same as table 3, but for the $z_{abs}=0.8526$ system in Q1330-2056 with $N_{H\ I}=19.40\pm 0.02$.

v	b_{eff}	Al III	Mg I	Mg II	Fe II
-439	6.2	(6.39±1.74)E11	-	>9.07E12	(2.23±0.37)E12
-365	9.9	(1.91±0.23)E12	(1.80±0.40)E11	>3.09E13	(8.13±0.50)E12
-295	4.3	-	-	(1.44±0.28)E12	-
-262	6.4	-	(1.03±0.35)E11	(2.23±0.30)E12	-
-192	9.7	(6.60±1.96)E11	(2.84±4.28)E11	>2.05E13	(6.50±0.47)E12
-121	7.2	-	-	(2.28±0.33)E12	-
-101	10.4	-	(2.07±0.43)E11	>5.25E12	(1.26±0.42)E12
-74	12.8	-	-	>3.49E12	(1.56±0.46)E12
-10	10.9	-	-	(2.31±0.31)E12	-
21	9.2	-	(2.97±0.43)E11	>2.91E13	(9.65±0.52)E12
46	10.4	-	(1.17±0.41)E11	>3.83E12	-
67	11.4	-	(1.09±0.41)E11	>6.20E12	(3.02±0.47)E12
99	7.5	-	(4.30±0.48)E11	>2.74E13	(1.75±0.07)E13
119	7.9	-	(1.58±0.41)E11	>7.84E12	(7.74±0.50)E12
136	6.4	(6.36±1.78)E11	(1.12±0.38)E11	>1.04E13	(4.31±0.42)E12

This system appears to have a super-solar abundance, with $[Zn/H]>+0.86$ and based on Fe II, the metallicity is $[Fe/H]>-0.07$. As was mentioned in § 4.2, the $[Fe/H]$ may be lower than this due to ionisation corrections. This system also shows a super-solar abundance in both Mn with $[Mn/H]>+0.15$ and Si with $[Si/H]>+0.68$. If the Mg I contribution to the blended Zn II + Mg I λ 2026 line is substantially more than what we have estimated based on the Mg I λ 2852 line, then the Zn II metallicity could be overestimated. However, the component structure of Mg I λ 2852 does not suggest that an Mg I λ 2026 blend could affect the detected dominant Zn II λ 2026 component. With such a low H I column density, it is possible that a substantial ionisation correction factor is needed for this system. The Al III/Al II ratio which can be used to estimate ionisation, could not be determined for this system as the Al II λ 1670 was not covered. Even with -1.0 dex ionisation corrections lowering the abundances, this system would still be well above the average metallicity of DLAs. Figure 9 gives velocity plots of several lines of interest. We give the results of the profile fitting analysis in table 12, along with the rest frame equivalent widths for the lines in this system in table 2.

4.8 Q1455-0045 ($z_{em}=1.378$)

(System A: $z_{abs}=1.0929$): There is a sub-DLA system with $\log N_{H\ I}=20.08\pm 0.06$ in the spectrum of this QSO (Rao, Turnshek, & Nestor 2006). We detected strong absorption lines from Mg I, Mg II, Al II, Al II, Si II, and Fe II in this system. A total of 10 components were used in the Voigt profile fits. No Zn II $\lambda\lambda$ 2026, 2062 lines were detected at $S/N\sim 27$ in the region. We could constrain the metallicity based on Zn as $[Zn/H]<-0.80$. The abundances based on the Fe II and Si II lines are $[Fe/H]=-0.98\pm 0.06$ and $[Si/H]=-0.98\pm 0.12$. The Mn II λ 2576 was also detected with $[Mn/H]=-1.43$ and $[Mn/Fe]=-0.51\pm 0.15$. We did detect both the Al II and Al III lines, with the ratio of column densities Al III/Al II <-0.18 . Weak features of Cr II λ 2056 were also detected with $W_0=21\pm 7$ mÅ. Only one component at ~ 64 km s $^{-1}$ was above a 3σ significance level with $[Cr/Fe]=-0.35\pm 0.13$, although another component at

~ 44 km s $^{-1}$ was at the $\sim 2\sigma$ level. The Cr II column density was found to be higher via the AOD method, with $[Cr/Fe]=0.0$. Figure 10 shows velocity plots of several lines of interest. We show the results of the profile fitting analysis in table 13, and the rest frame equivalent widths for this system in table 2.

5 DISCUSSION AND CONCLUSIONS

The abundances for the observed systems are given in table 14. We have used the total column densities (i.e. the sum of the column densities in the individual components of a system that were determined via profile fitting method) along with the total $N_{H\ I}$ as given in table 1, to determine the abundances of these systems. It would be interesting to determine the abundances in the individual components, as they may possibly vary from component to component. This however is impossible at the present time due to the lack of high resolution UV spectrographs that would be necessary to determine $N_{H\ I}$ in individual components. We have ignored any ionisation corrections while determining these abundances, and have assumed the first ions to be the dominant ionisation species of the elements for which these abundances have been determined, namely Zn, Fe, Mn, Cr, and Si. We discuss the issue of ionisation further below. Solar systems abundances from Lodders (2003) are also given in table 14. The abundances for Ca II are likely only lower limits, as the ionisation potential of 11.868 eV for Ca $^+$ is lower than ionisation potential of H 0 (13.6 eV).

Relative abundances of various elements are also given in table 14, with the column densities determined from the profile fitting analysis. We give the metallicities of these systems, along with the $[Zn/Fe]$ ratio, which is often used as an indicator of dust depletion. We also provide the ratios of $[Si/Fe]$, $[Ca/Fe]$, $[Cr/Fe]$, and $[Mn/Fe]$. Finally, we provide ratios of the column densities of the adjacent ions Al III/Al II and Mg II/Mg I as well as Mg II/Al III and Fe II/Al III, any of which may provide information about the ionisation in these systems. By matching the observed ratios of the ions mentioned above to those generated through grids of photoionisation models, one can constrain the levels of ionisation, and any ionisation correction factors for the observed abundances.

Based on grids of Cloudy models, it has previously been

Table 11. Same as table 3, but for the $z_{abs}=0.7377$ system in Q1436-0051 with $N_{H\ I}=20.08\pm 0.11$.

v	b_{eff}	Mg I	Mg II	Ca II	Mn II	Fe II	Zn II
-49	3.6	-	$>1.00E13$	-	$(4.40\pm 1.07)E11$	-	-
-34	13.2	$(6.65\pm 0.76)E11$	$>8.68E13$	$(4.18\pm 1.37)E11$	$(2.18\pm 0.21)E12$	$(1.56\pm 0.06)E14$	-
-25	3.5	$(2.67\pm 0.81)E11$	-	-	$(6.66\pm 1.53)E11$	$(2.09\pm 0.12)E13$	-
-11	11.1	$>2.51E12$	$>5.74E13$	$(2.69\pm 0.17)E12$	$(4.11\pm 0.19)E12$	$(3.82\pm 0.33)E14$	$(2.17\pm 0.49)E12$
19	11.5	$>3.48E12$	$>7.13E13$	$(2.61\pm 1.68)E12$	$(2.47\pm 0.16)E12$	$(2.70\pm 0.16)E14$	$(1.74\pm 0.17)E12$
35	5.6	$>1.31E12$	$>2.26E13$	$(9.22\pm 1.25)E12$	$(4.29\pm 1.12)E11$	$(3.00\pm 0.34)E13$	$(7.16\pm 1.36)E11$
47	5.7	$(1.15\pm 0.36)E11$	$>1.23E13$	-	-	$(6.94\pm 0.71)E12$	-
62	8.0	-	$(4.03\pm 0.21)E12$	-	-	$(2.24\pm 0.52)E12$	-

Table 12. Same as table 3, but for the $z_{abs}=0.9281$ system in Q1436-0051 with $N_{H\ I} < 18.8$.

v	b_{eff}	Mg I	Mg II	Al III	Si II	Ca II	Mn II	Fe II	Zn II
-70	6.8	-	$(1.70\pm 0.37)E12$	-	-	-	-	-	-
-44	6.6	-	$(3.00\pm 0.51)E12$	-	-	-	-	-	-
-14	2.7	-	$>1.09E15$	$(4.62\pm 0.93)E12$	-	-	$(4.64\pm 1.82)E11$	$(8.56\pm 1.00)E12$	-
9	10.7	$(2.79\pm 0.28)E12$	$>9.99E13$	$(1.83\pm 0.14)E13$	$(1.04\pm 0.13)E15$	$(1.89\pm 0.16)E12$	$(2.36\pm 0.27)E12$	$(1.30\pm 0.05)E14$	$(1.97\pm 0.27)E12$
36	7.3	-	$>1.61E13$	$(1.03\pm 0.33)E12$	-	-	-	$(6.91\pm 0.70)E12$	-
60	8.0	$(2.86\pm 0.75)E11$	$>1.15E14$	$(1.17\pm 0.33)E12$	-	-	-	$(1.26\pm 0.08)E13$	-

shown that there appears to be little need for ionisation corrections in most sub-DLA systems (Dessauges-Zavadsky et al. 2003; Meiring et al. 2007). We have therefore not applied any ionisation corrections to the abundances in table 14. We do note however, that the $z_{abs}=0.8301$ system with $N_{H\ I}=18.95\pm 0.18$ in Q1054-0020 and the $z_{abs}=0.9281$ system with $N_{H\ I} < 18.8$ in Q1436-0051 both show possible signs of high levels of ionization, with Fe II/Al III=0.74 and Fe II/Al III=0.80 respectively. Substantial ionisation corrections could be necessary. Cloudy models for the $z_{abs}=0.9281$ system in Q1436-0051 indicate a positive ionization correction factor for Zn in this system of $\sim +0.2$ to $+0.3$ dex for $-6 < \log U < -3$ (indicating that $[Zn\ II/H\ I]$ underestimates the true abundance by this amount). We caution that these results may be inaccurate due to uncertainties in the atomic data for Zn. The ionisation correction factors for Si, Mn, and Fe are all negative over this range of ionisation parameters with values of ~ -0.3 to -0.5 dex for Mn and Fe, and values ranging from ~ 0.0 to ~ -1.25 for Si. Based on these models, it appears that $[Fe/Zn]$ is suppressed as one goes to lower and lower $N_{H\ I}$ values, the true depletion is actually much higher than it appears based on Zn II and Fe II. Similar values were derived for the $z_{abs}=0.8301$ system with $N_{H\ I}=18.95\pm 0.18$ in Q1054-0020 based on Cloudy models. As no adjacent ions that could constrain the ionisation parameter are available for these systems, we leave the abundances unaltered in table 14. We prefer to leave the corrections to a later time when more constraints are available (i.e. when we have UV spectra with coverage of Fe III, S III, Si IV, etc and better atomic data become available).

Variations by component of the relative abundances of elements can also provide information about the local star formation history and possibly ionization. Prochaska et al. (2002) noticed a remarkably small (~ 0.3 dex) component-by-component dispersion in $[Zn/Fe]$ over a wide range of metallicities. As we only have Zn detections for two of the systems here, we instead look at $[Mn/Fe]$, which is likely less affected by dust depletion (Mn and Fe have similar condensation temperature) and more affected by nucleosynthetic enrichment. Unfortunately, other ions such as Mg

II and Al II are too saturated to determine accurate column densities in most of the individual components. The $z_{abs}=1.4244$ system in Q1037+0028 and the $z_{abs}=0.8301$ system in Q1054-0020 show similarly low dispersions of $[Mn/Fe]$, but interestingly the high metallicity $z_{abs}=0.7377$ and $z_{abs}=0.9281$ systems of Q1436-0051 show higher spreads of $[Mn/Fe]$ of ~ 0.6 and ~ 0.5 dex respectively. The metal rich sub-DLA observed in Péroux et al. (2006a) also showed a large dispersion in $[Mn/Fe]$. The $z_{abs}=0.7377$ system in Q1436-0051 also shows a 0.6 dex range of $[Zn/Fe]$ in the components. One possible explanation for these larger dispersions could be enrichment by recent supernovae explosions in which the gas has not had time to sufficiently mix.

Zn II was detected in only 2 of the systems, and upper limits on the Zn abundance were placed on the rest of the systems. The Cr II λ 2056 line was detected only in the $z_{abs}=1.0929$ system in Q1455-0045. Due to the weakness of the Lyman- α line in the $z_{abs}=0.9281$ system in Q1436-0051, only an upper limit could be placed on the neutral hydrogen column density, and therefore lower limits on the abundances in this system. This system shows an unusual abundance pattern, with high metallicity ($[Zn/H] > +0.86$, $[Fe/H] > -0.07$, and $[Si/H] > +0.68$) and high depletion ($[Zn/Fe] = +0.94$). This system also showed an overabundance of Mn, with $[Mn/Fe] = +0.22$. As Mn is an odd element, and Fe is even, $[Mn/Fe]$ might be below solar in material whose source is dominated by the products of Type II supernovae, but likely not higher if differential dust depletion effects are negligible. In the other case of a Zn detection, the system at $z_{abs}=0.7377$ in Q1436-0051, Mn is also slightly more abundant relative to Fe, with $[Mn/Fe] = +0.04$. Ledoux, Bergeron, & Petitjean (2002) found a large dispersion in $[Mn/Fe]$ based on a sample of DLA absorbers and concluded that this large range of values not seen in other abundance ratios such as $[Cr/Fe]$ or $[Si/Fe]$ must be due to a combination of both depletion and nucleosynthetic effects.

A similar over-abundance of Mn relative to Fe was also seen by Péroux et al. (2006a) in another sub-DLA at $z_{abs}=0.716$ with $[Zn/H] = +0.61$ and $[Mn/Fe] = +0.14$. This could perhaps be due to

Table 13. Same as table 3, but for the $z_{abs}=1.0929$ system in the spectrum of Q1455-0045 with $N_{\text{H I}}=20.08\pm 0.06$.

v	b_{eff}	Mg I	Mg II	Al II	Al III	Si II	Cr II	Mn II	Fe II
-95	8.8	-	(1.00±0.09)E12	-	(4.92±1.51)E11	-	-	-	-
-60	9.8	(3.01±0.50)E11	>2.02E14	>7.21E12	(2.87±0.22)E12	-	-	-	(2.15±0.09)E13
-42	7.5	(7.42±0.78)E11	>8.96E12	>3.09E12	(2.46±0.23)E12	-	-	(1.23±0.40)E12	(3.64±0.20)E13
-30	8.2	(4.12±0.59)E11	>1.33E14	>7.51E12	(2.37±0.22)E12	-	-	-	(5.02±0.22)E13
3	10.3	(1.81±0.55)E11	>1.10E14	>1.62E13	(1.06±0.05)E13	-	-	-	(4.73±0.19)E13
15	7.1	(2.95±0.65)E11	>1.05E13	>5.51E12	(4.69±0.50)E12	-	-	-	(2.24±0.20)E13
26	8.1	-	>2.20E13	>1.80E12	(2.03±0.30)E12	-	-	-	(1.51±0.13)E13
45	11.1	(4.89±0.59)E11	>7.02E13	>1.67E12	(9.50±0.44)E12	-	-	-	(6.78±0.26)E13
64	7.9	(6.30±0.71)E11	>5.66E13	>3.05E12	(7.52±0.46)E12	-	(2.51±0.71)E12	-	(6.66±0.38)E13
77	8.8	(2.17±0.53)E11	>2.18E14	>6.12E12	(2.56±0.25)E12	(4.40±0.10)E14	-	-	(4.65±0.21)E13

heavy depletion of Fe compared to Mn onto dust grains, unmixed gas that has recently been expelled through stellar winds and supernovae, or an intrinsically non-solar abundance pattern. Cloudy models for this system indicate that the corrections for $[\text{Mn}/\text{Fe}]$ due to ionisation are small ($\lesssim 0.10$ dex for $-6 < \log U < -1$). In the other 3 cases where we have detections of Mn and Fe, but no Zn, Mn is slightly under-abundant relative to Fe, with $\langle [\text{Mn}/\text{Fe}] \rangle = -0.31$. The systems in our sample have an average Fe abundance of $\langle [\text{Fe}/\text{H}] \rangle = -0.68$, which is higher than for typical DLA systems ($\langle [\text{Fe}/\text{H}] \rangle_{\text{DLA}} \sim -1.5$). This may be due to less dust depletion or truly higher abundances in these systems, or to undue influence of ionisation effects in the low $N_{\text{H I}}$ systems.

To determine an average $[\text{Zn}/\text{H}]$ abundance of the absorbers in this sample, the spectra were shifted to rest wavelengths and averaged. Any obvious non-associated features in the region around the Zn II λ 2026 line in the individual spectra were replaced by random noise with S/N similar to the uncontaminated regions. We show the average spectrum around Zn II λ 2026 Å in Figure 11. A feature was seen in the region with $W_0=8\pm 2$ mÅ and $\log N_{\text{Zn II}}=11.63$. The feature at $\sim +70$ km s $^{-1}$ may be due to absorption from Mg I λ 2026.477, and was not included when determining W_0 . The systems in this sample have an average H I column density of $\log \langle N_{\text{H I}} \rangle = 19.80$, giving this sample an average Zn abundance of $\langle [\text{Zn}/\text{H}] \rangle = -0.80$ based on this composite spectrum. To increase the S/N, we also binned the averaged spectrum to a dispersion of 0.5 Å/pixel ($R \sim 4000$). After binning, a feature was detected at a $\gtrsim 2\sigma$ significance level with $W_0=11$ mÅ. If the feature is assumed to be a true detection, the Zn II column density is $\log N_{\text{Zn II}}=11.80$, with a corresponding mean abundance of $\langle [\text{Zn}/\text{H}] \rangle = -0.63$ for these absorbers at $0.7 \lesssim z_{abs} \lesssim 1.5$ based on the binned spectrum. In comparison, DLA absorbers have a mean Zn abundance of $\langle [\text{Zn}/\text{H}] \rangle \sim -1.0$ in this redshift range (Kulkarni et al. 2005, 2007).

The $N_{\text{H I}}$ -weighted mean metallicity given by:

$$[\langle X/\text{H} \rangle] = \log \langle (X/\text{H}) \rangle - \log (X/\text{H})_{\odot} \quad (2)$$

where

$$\langle (X/\text{H}) \rangle = \frac{\sum_{i=1}^n N(X)_i}{\sum_{i=1}^n N(\text{H})_i} \quad (3)$$

has often been used as a quantitative way of estimating the amount of metal enrichment in the Universe in a given epoch (Kulkarni et al. 2005, 2007). For the absorption systems in this sample, the $N_{\text{H I}}$ -weighted mean metallicity based on Fe is $\langle [\text{Fe}/\text{H}] \rangle = -0.76$. Using Zn which is less affected by dust depletion, we determine the $N_{\text{H I}}$ -weighted mean metallicity for these

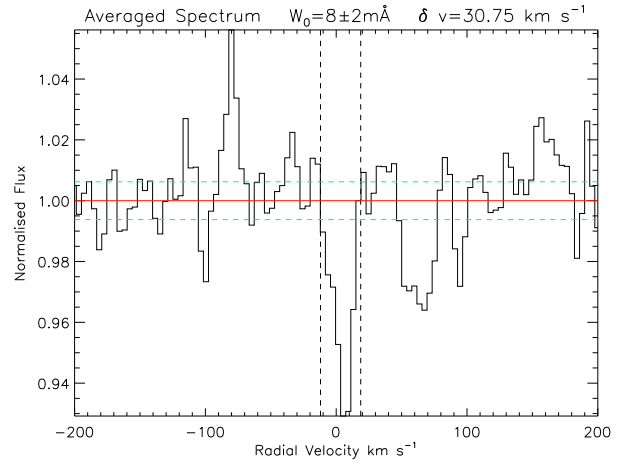


Figure 11. The unbinned average spectrum of the 10 absorbers in this sample near Zn II λ 2026 Å. The horizontal red line indicates the continuum level, and the horizontal dashed green lines show the best fit continuum level increased or decreased by $\pm 40\%$ of the RMS variance in the noise. The vertical dashed lines show the integration limits. The feature seen was detected at $\gtrsim 4\sigma$ with $W_0=8\pm 2$ mÅ.

systems at $0.7 \lesssim z_{abs} \lesssim 1.5$, to be $\langle [\text{Zn}/\text{H}] \rangle = -0.40$ assuming the upper limits to be detections, and $\langle [\text{Zn}/\text{H}] \rangle = -0.70$ assuming the limits to be zero.

In this paper we have presented medium-resolution spectra of 10 sub-DLAs at $z_{abs} \lesssim 1.5$. Although to date the DLA systems have been the preferred tracer of metallicity at high redshift, every absorber with solar or higher metallicity that has been detected has been a sub-DLA (Pettini et al. 2000; Khare et al. 2004; Péroux et al. 2006a; Prochaska et al. 2006; Meiring et al. 2007). With this latest sample of sub-DLAs, we have found two more systems with high metallicity, $[\text{Zn}/\text{H}] = -0.05$ and $[\text{Zn}/\text{H}] > +0.86$. Two other systems in this sample that did not have a Zn II detection, did nonetheless have $[\text{Fe}/\text{H}] > -0.30$.

These observations suggest that the largely ignored sub-DLAs may provide important clues into the chemical evolution of the Universe. Clearly, not all sub-DLAs have solar or higher metallicity, nor would one expect them to if they trace typical galaxies which have a range of metallicities. Sub-DLAs do appear, however, to have a higher mean metallicity and show faster evolution than do DLAs (Kulkarni et al. 2007). We continue to find systems with low $N_{\text{H I}}$ and high metallicities, but higher S/N is needed to determine if the systems with upper limits of $[\text{Zn}/\text{H}] \sim -0.3$ are indeed at that

level, or are much less, comparable to DLA abundances. With our sample sizes of sub-DLAs now increasing, we can begin to address some of the questions relating to the chemical evolution of metals. Future UV spectra would also allow measurements of key lines of S III and Fe III which could yield important information about ionisation. In forthcoming work, and with an extended sample, we will examine differences in the properties of sub-DLAs and DLAs, including abundances and kinematical structure, as well as the redshift evolution of these properties in sub-DLAs.

ACKNOWLEDGMENTS

We thank the helpful staff of Las Campanas Observatory for their assistance during the observing runs. J. Meiring and V.P. Kulkarni gratefully acknowledge support from the National Science Foundation grant AST-0607739 (PI Kulkarni). J. Meiring acknowledges partial support from a South Carolina Space Grant graduate student fellowship.

APPENDIX - $N_{\text{H I}}$ DETERMINATIONS

The systems studied in this work all have known $N_{\text{H I}}$ from HST spectra. For completeness and convenience to the reader, we provide plots of the Voigt profiles of the Lyman- α transition using the best fit values of the column density from Rao, Turnshek, & Nestor (2006). Due to the low resolution and S/N of these UV spectra, only one component was used in the fits. We show in figures A1 through A10 the Voigt profiles corresponding to the column densities given by Rao, Turnshek, & Nestor (2006) and convolved with a Gaussian instrumental spread function based on a two pixel resolution element, superimposed on the archival data from HST cycle 6 program 6577, cycle 9 program 8569, and cycle 11 program 9382. We note that the normalization, i.e., the continuum fit that we define may differ from that adopted by Rao, Turnshek, & Nestor (2006). For our continuum fits, a polynomial typically of order 5 or less or a cubic spline was used, and the absorption line itself was excluded from the fitting region. Also over-plotted are profiles with H I column densities smaller and larger by 0.15 dex than the best fit values. For the $z_{\text{abs}}=0.7377$ system in Q1436-0051 in which the $N_{\text{H I}}$ value is given as an upper limit, we plot this value ($\log N_{\text{H I}}=18.8$), along with profiles with H I column densities smaller and larger by 0.15 dex.

A horizontal bar in the middle of the profile or directly beneath it denotes the region in velocity space where Mg II absorption was seen. This spread in Mg II absorption is likely a lower limit of the spread in H I, as some components could have detectable H I without detectable Mg II. It should be noted that it is possible that $N_{\text{H I}}$ may be overestimated when using only one component to fit the profiles. Multiple components spread over the width of absorption seen in Mg II may decrease the total $N_{\text{H I}}$ needed to fit the profile, and thus increase the abundances. Higher resolution UV spectra covering higher Lyman series transitions would help to resolve the effects of the wide spread of the Mg II components, and discern abundance differences between components which is not possible with the current lower resolution UV spectra.

REFERENCES

Barthel P.D., Tytler D.R., Thompson B., 1990, *A&AS*, 82, 339
Bergeron J., Kunth D., D’Odorico S., 1987, *A&A*, 180, 1

Bernstein R., Schectman S.A., Gunnels S., Mochnacki S., Athey A., 2003 *SPIE*, 4841, 1694
Chen H-W., Lanzetta K.M., 2003, *ApJ*, 597, 706
Charlton J.C., Ding J., Zonak S.G., Churchill C.W., Bond N.A., Rigby J.R., 2003, *ApJ*, 589, 111
Dessauges-Zavadsky M., Peroux C., Kim T.S., D’Odorico S., McMahon R.G., 2003, *MNRAS*, 345, 447
Ding J., Charlton J.C., Churchill C.W., Palma C., 2003, *ApJ*, 590, 746
Ellison, S., 2006, *MNRAS*, 368, 355
Fang T., Marshall H.L., Lee J.C., Davis D.S., Canizares C.R., 2002, *ApJ*, 527, 127
Herbert-Fort S., Prochaska J.X., Dessauges-Zavadsky M., Ellison S.L., Howk J.C., Wolfe A.M., Prochter G.E., 2006, *PASP*, 118, 1077
Hewitt A., Burbidge G., 1987, *ApJS*, 63, 1
Khare P., Kulkarni V.P., Lauroesch J.T., York D.G., Crofts P.S., Nakamura O., 2004, *ApJ*, 616, 86
Khare P., Kulkarni V.P., Péroux C., York D.G., Lauroesch J.T., Meiring J.D., 2007, *A&A*, 464, 487
Kulkarni V.P., Hill J.M., Schneider G., Weymann R.J., Storrie-Lombardi L.J., Rieke M.J., Thompson R.I., Jannuzi B.T., 2000, *ApJ*, 536, 36
Kulkarni V.P., Hill J.M., Schneider G., Weymann R.J., Storrie-Lombardi L.J., Rieke M.J., Thompson R.I., Jannuzi B.T., 2001, *ApJ*, 551, 37
Kulkarni V.P., Fall S.M., Lauroesch J.T., York D.G., Welty D.E., Khare P., Truran J.W., 2005, *ApJ*, 618, 68
Kulkarni V.P., Khare P., Péroux C., York D.G., Lauroesch J.T., Meiring J.D., 2007, *ApJ*, 661, 88
Kunth D., Bergeron J., 1984, *MNRAS*, 210, 873
Lanzetta K. M., Turnshek D. A., Wolfe A. M., 1987, *ApJ*, 322, 739
Lauroesch J.T., Truran J.W., Welty D.E., York D.G., 1996, *PASP*, 108, 726
Lodders, K., 2003, *ApJ*, 591, 1220
Ledoux C., Bergeron J., Petitjean P., 2002, *A&A*, 385, 802
Masiero J.R., Charlton J.C., Ding J., Churchill C.W., Kacprzak G., 2005, *ApJ*, 623, 57
Meiring J.D., Kulkarni V.P., Khare P., Bechtold J., York D.G., Cui J., Lauroesch J.T., Crofts A.P.S., Nakamura O., 2006, *MNRAS*, 370, 43
Meiring J.D., Lauroesch J.T., Kulkarni V.P., Péroux C., Khare P., York D.G., Crofts A.P.S., 2007, *MNRAS*, 376, 557
Morton D.C., 2003, *ApJS*, 149, 205
Nestor D.B., Rao S.M., Turnshek D.A., Vanden Berk D., 2003, *ApJ*, 595, L5
Nestor D. B. 2004, Ph.D. thesis, Univ. Pittsburgh
Nissen P. E., Chen Y. Q., Asplund M., Pettini M., 2004, *A&A*, 415, 993
Péroux C., Storrie-Lombardi L., McMahon R., Irwin M., & Hook I., 2001, *AJ*, 121, 1799
Péroux C., Dessauges-Zavadsky M., D’Odorico S., Kim T.S., McMahon R., 2003, *MNRAS*, 345, 480
Péroux C., McMahon R.G., Storrie-Lombardi L.J., Irwin M.J., 2003, *MNRAS*, 346, 1103
Péroux C., Kulkarni V.P., Meiring J., Ferlet R., Khare P., Lauroesch J.T., Vladilo G., York D.G., 2006, *A&A*, 450 53
Péroux C., Meiring J., Kulkarni V.P., Ferlet R., Khare P., Lauroesch J.T., Vladilo G., York D.G., 2006, *MNRAS*, 372, 369
Petitjean P., Webb J.K., Rauch M., Carswell R.F., Lanzetta K., 1993, *MNRAS*, 262, 499

Table 14. Relative abundances and abundance ratios for the observed sub-DLAs. The first line below the heading gives the solar reference abundance for that column.

QSO	z_{abs}	Log N _{H I}	[Zn/H]	[Fe/H]	[Zn/Fe]	[Si/Fe]	[Ca/Fe]	[Cr/Fe]	[Mn/Fe]	Al III/Al II ^a	Mg II/Mg I ^a	Mg II/Al III ^a	Fe II/Al II
[X/Y] _☉			-7.37	-4.53	-2.85	+0.07	-1.13	-1.82	-1.97				
Q1037+0028	1.4244	20.04±0.12	< -0.63	-0.67±0.12	< +0.04	0.18±0.04	-	< -0.76	-0.34±0.05	< -0.96	-	>2.29	1.65±0.0
Q1054-0020A	0.8301	18.95±0.18	< +0.18	-0.09±0.18	< +0.28	-	-	< -0.04	-0.09±0.07	-	>2.28	>1.24	0.74±0.0
Q1054-0020B	0.9514	19.28±0.02	< -0.21	-1.09±0.02	< +0.88	< +0.52	-	< +0.36	< +0.23	-	>1.68	>1.61	>1.55
Q1215-0034	1.5543	19.56±0.02	< -0.56	-0.64±0.02	< +0.08	-	-	< -0.20	< -0.79	-	-	-	-
Q1220-0040	0.9746	20.20±0.07	< -1.14	-1.33±0.07	< +0.19	-	-	< -0.14	< -0.42	-	>2.69	>2.19	1.72±0.0
Q1228+1018	0.9376	19.41±0.02	< -0.37	-0.30±0.02	< -0.07	-	-	< -0.55	< -0.47	-	>2.29	-	-
Q1330-2056	0.8526	19.40±0.02	< -0.07	-1.07±0.02	< +1.00	-	-	< +0.20	< -0.22	-	>1.88	>1.62	1.21±0.0
Q1436-0051A	0.7377	20.08±0.11	-0.05±0.12	-0.61±0.11	+0.58±0.04	-	-0.98±0.03	< -0.41	+0.04±0.03	-	-	-	-
Q1436-0051B	0.9281	<18.8	>+0.86	> -0.07	+0.94±0.06	+0.75±0.05	-0.79±0.04	< +0.20	+0.22±0.05	-	>2.63	>1.72	0.80±0.0
Q1455-0045	1.0929	20.08±0.06	< -0.80	-0.98±0.06	< +0.18	+0.00±0.10	-	-0.35±0.13	-0.51±0.15	< -0.18	>2.39	>1.27	0.92±0.0

^aRatios of column densities

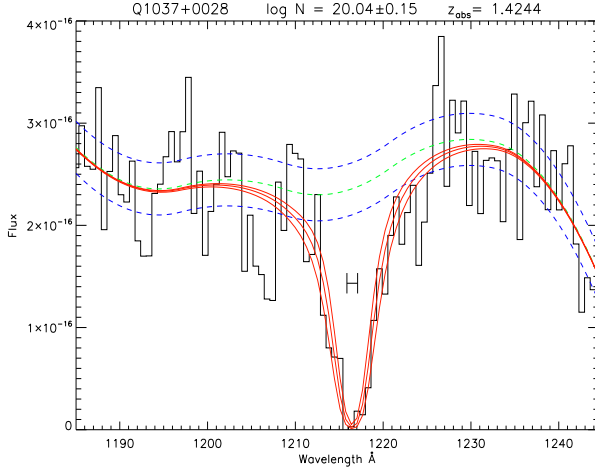
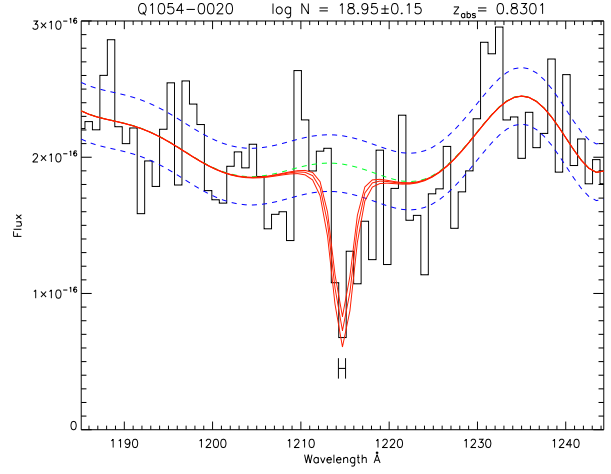
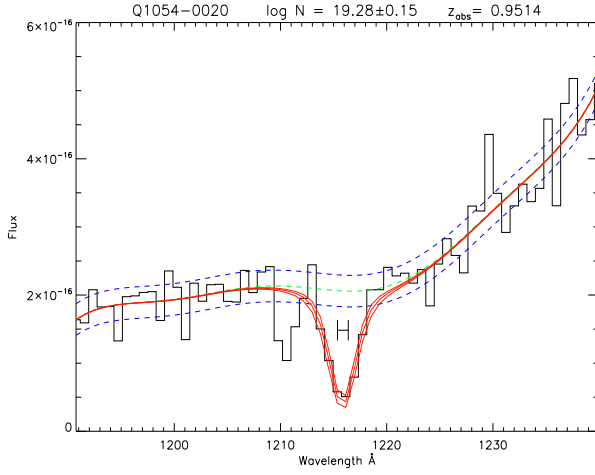
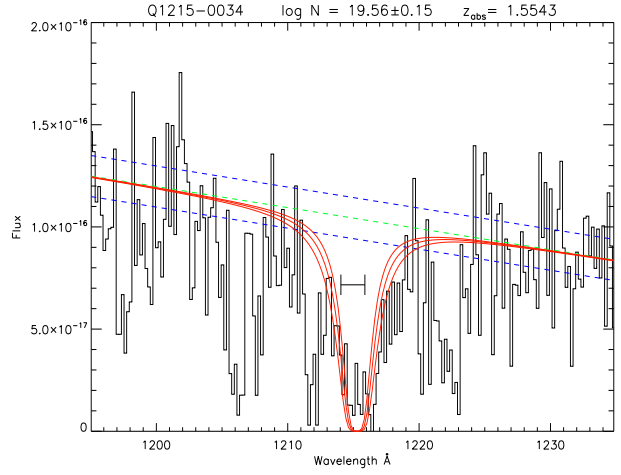
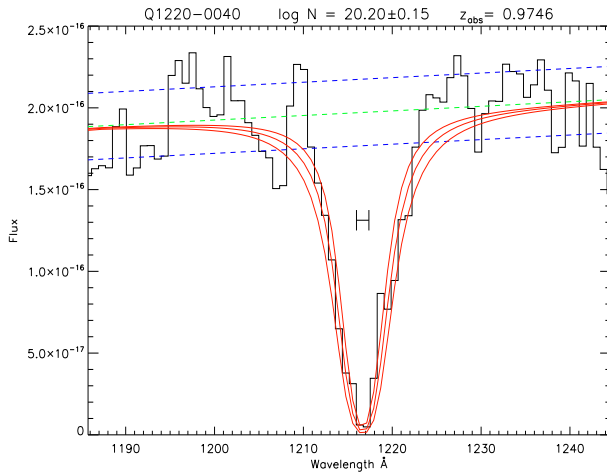
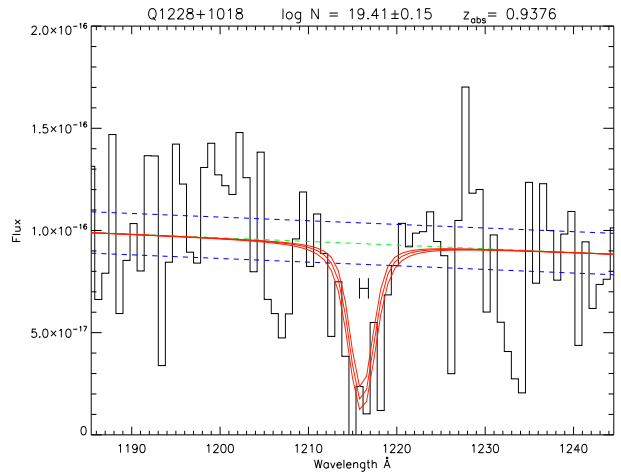

Figure A1.

Figure A2.

Figure A3.

Figure A4.

Figure A5.

Figure A6.

Figure A1 - A6: UV spectra of the systems (clockwise from top left) $z_{abs}=1.4244$ in Q1037+0038, $z_{abs}=0.8301$ in Q1054-0020, $z_{abs}=1.5543$ in Q1215-0034, $z_{abs}=0.9376$ in Q1228+1018, $z_{abs}=0.9746$ in Q1220-0040 and $z_{abs}=0.9514$ in Q1054-0020. The dashed green line indicates the best fit level of the continuum, and the dashed blue lines are increased or decreased by 10% of the best fit value. Superimposed on the data are theoretical Voigt profiles that have been convolved with a gaussian instrumental spread function. The middle profile is the best fit value from Rao, Turnshek, & Nestor (2006), and the upper and lower column densities have been modified by ± 0.15 dex from the best fit value. The horizontal bar either in the center of the profile or directly beneath the line center denotes the region in velocity space where Mg II absorption is seen.

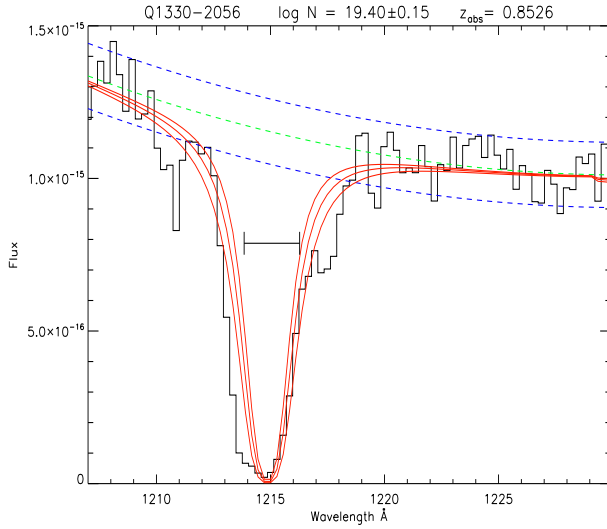


Figure A7.

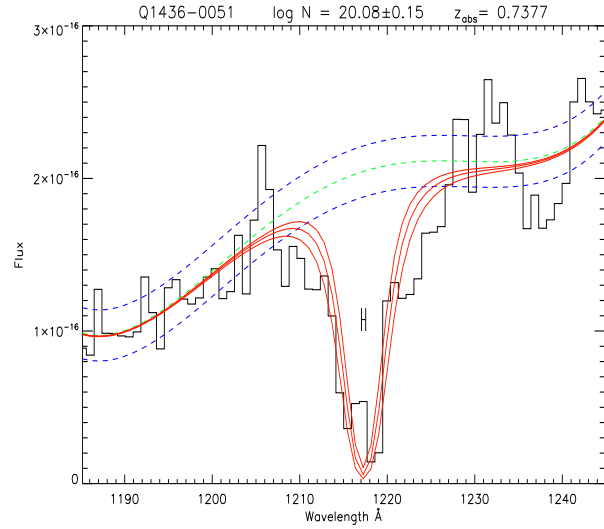


Figure A8.

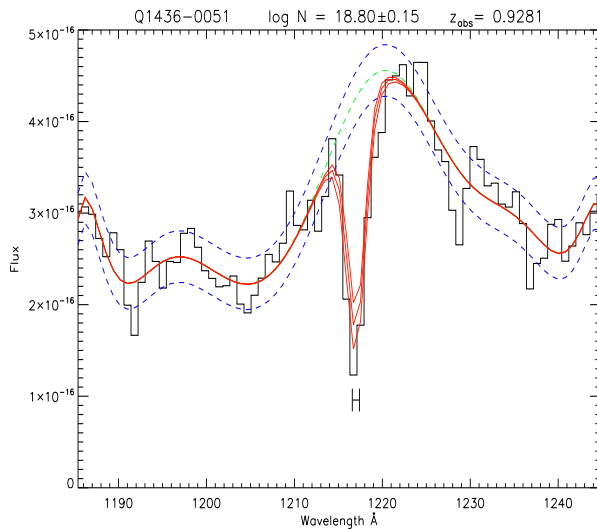


Figure A9.

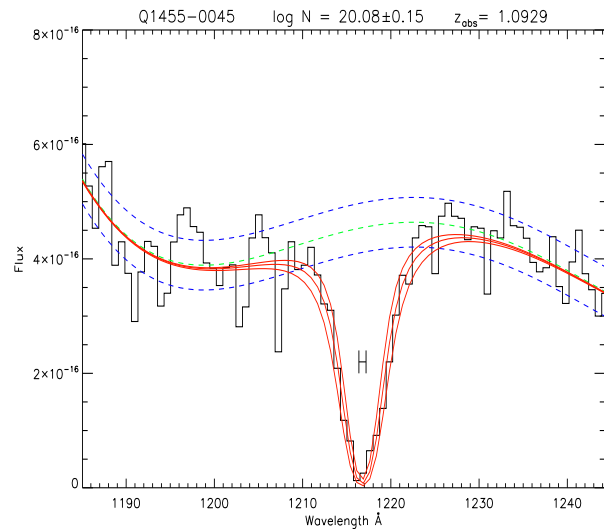


Figure A10.

Figure A7 - A10: Same as Figures 11-16, but for the systems (clockwise from top left) $z_{abs}=0.8526$ in Q1330-2056, $z_{abs}=0.7377$ in Q1436-0051, $z_{abs}=1.0929$ in Q1455-0045, and $z_{abs}=0.9281$ in Q1436-0051.

Pettini M., Ellison S.L., Steidel C.C., Shapley A.E., Bowen, D.V., 2000, *ApJ*, 532, 65
 Prochaska J.X., Wolfe A.M., 2002, *ApJ*, 566, 68
 Prochaska J.X., Howk J.C., O'Meara J.M., Tytler D., Wolfe A.M., Kirkman D., Lubin D., Suzuki N., 2002, *ApJ*, 571, 693
 Prochaska J.X., O'Meara J.M., Herbert-Fort S., Burles S., Prochter G.E., Bernstein R.A., 2006, *ApJ*, 648, 97
 Rao S.M., Turnshek D.A., Nestor D.B., 2006, *ApJ*, 636, 610
 Rao, S.M., Nestor, D.B., Turnshek, D.A., Lane, W.M., Monier, E.M., Bergeron, J., 2003, *ApJ*, 595, 94
 Richards G.T., Fan X., Schneider D.P., Vanden Berk D.E., Strauss M.A., York D.G., Anderson J.E., Anderson S.F., 2001, *AJ*, 121, 2308
 Sargent W. L. W., Steidel C. C., Boksenberg A., 1989, *ApJS*, 69, 703
 Savage B.D., Sembach K.R., 1996, *ApJ*, 379, 245
 Simcoe R.A., Sargent W.L.W., Rauch M., 2002, *ApJ*, 578, 737
 Schaye J., Carswell, R.F., Kim, T., 2007, *MNRAS* 379, 1169

Vidal-Madjar A., Laurent C., Bonnet R. M., York D. G., 1977, *ApJ*, 211, 91
 Welty D.E., Hobbs L.M., York D.G., 1991, *ApJS*, 75, 425
 York D.G., Khare P., Vanden Berk D., Kulkarni V.P., Crofts A.P.S., Lauroesch J.T., Richards G.T., et al., 2006, *MNRAS*, 367, 945

This paper has been typeset from a $\text{\TeX}/\text{\LaTeX}$ file prepared by the author.